

Light-Activated Liquid Crystalline Hierarchical Architecture Toward Photonics

Ling-Ling Ma, Wei Hu, Zhi-Gang Zheng, Sai-Bo Wu, Peng Chen, Quan Li,* and Yan-Qing Lu*

Hierarchical architectures are of vital importance in materials science and nanotechnology. Among various building blocks, liquid crystals (LCs) have attracted particular attention due to their excellent controllability of self-assembly behavior and the resultant physical properties. In recent years, interest in light-activated LC hierarchical superstructures has emerged for a wide range of applications beyond LC displays. This report consists of two main parts: the light-activated LC hierarchical architectures and their corresponding photonic applications. In the first part, different smectic layer curvature controlling methods are introduced to produce periodic defect arrays. By taking the advantages of photoalignment techniques and light-driven molecular motors, cholesteric LC helical superstructures are highly manipulated, including pitch tuning, helix rotation, and chirality inversion. As a mutually concerned scientific issue, the photoresponsive properties of blue phase (BP) hierarchical superstructures are also introduced, enabling unique BP materials and devices driven by a facile light stimulation. Moreover, traditional optics (microlens and beam steering) and advanced photonics (specific optical field generation and LC lasers) are reviewed in the second part. It is believed that the developments introduced here can open a door for the concept of “*smart optical materials*” based on the self-assembled soft LC superstructures.

1. Introduction

Structures bridge the micro and macro worlds and play vital roles in material sciences and technologies. Nature is more wondrous than our imagination, which always solves complicated problems in simple manners. For instance, the iridescence in butterfly wings, peacock feathers, and opals;^[1] the self-cleaning ability of lotus leaves;^[2] the water-repellent legs of water striders;^[3] and the dry adhesion of gecko foot hairs^[4] are all resulted from exquisite structures with long-range ordered multiscale organizations; DNA can be considered as a nanoscale knotting structure for recording and reading genetic information. Such phenomena provide amounts of inspirations for the development of new functional materials via mimicking natural structures. Hierarchical architecture in the mesoscopic scale is a booming topic that triggers curiosities toward insights of fantastic natural materials. In recent years, much effort has been devoted to this field, and numerous novel artificial architectures have been presented.

Thanks to the intrinsic self-assembly behavior, liquid crystal (LC) is a promising candidate for building up ideal hierarchical superstructures. The molecular self-organization of LCs enables a landscape of hierarchical architectures featured by fantastic textures in diverse phases. Nematic LC is commonly composed of rod-like molecules with their long axes along a preferred direction (Figure 1A). Different LC director distributions would introduce varied anisotropic physical properties. The orientational order introduces various anisotropic physical properties. While some other LC phases allow the rational control of assembly behavior and cause the formation of remarkable hierarchical superstructures. Moreover, advantages of widely tunable feature size, extra-field tunability as well as rapid and cost-effective formation are exhibited. Smectic LCs (SLCs) are characterized by an ordered lamellar structure (Figure 1B).^[5] Within each layer, molecules align parallel to each other, with their long axes parallel or incline to the layer normal. Under antagonistic anchoring conditions (i.e., the two interfaces of the SLC film are introduced with a planar alignment and a homeotropic alignment, respectively), parallel layers periodically wrap around defect lines to form different defect arrays.^[6] The cholesteric LC (CLC) is an LC phase where rod-like molecules self-assemble into a periodic helical structure (Figure 1C). This


Dr. L.-L. Ma, Prof. W. Hu, S.-B. Wu, Dr. P. Chen, Prof. Y.-Q. Lu
National Laboratory of Solid State Microstructures
Key Laboratory of Intelligent Optical Sensing and Manipulation
Collaborative Innovation Center of Advanced Microstructures
and College of Engineering and Applied Sciences
Nanjing University
Nanjing 210093, China
E-mail: yqlu@nju.edu.cn

Prof. W. Hu, S.-B. Wu, Dr. P. Chen
Institute for Smart Liquid Crystals
JITRI

Changshu 215500, China

Prof. Z.-G. Zheng
Department of Physics
East China University of Science and Technology
Shanghai 200237, China

Prof. Q. Li
Liquid Crystal Institute and Chemical Physics Interdisciplinary Program
Kent State University
Kent, OH 44242, USA
E-mail: qli1@kent.edu

 The ORCID identification number(s) for the author(s) of this article can be found under <https://doi.org/10.1002/adom.201900393>.

DOI: 10.1002/adom.201900393

remarkable structure results in a helical-variant dielectric tensor, thus contributing to a natural 1D photonic crystal.^[7] It is endowed with a broadband Bragg reflection with a unique circular-polarization selectivity. Blue phase (BP) is another fantastic phase with 3D stacked lattice (Figure 1D).^[8] Such an elegant state-of-matter is energetically preferred in a high chirality system, commonly existing in a narrow temperature range of less than 1 K, between the cholesteric and isotropic phases. It has an exotic arrangement characteristic of LCs, which twists around two helical axes forming cylinders including hierarchically twisted molecular architectures. Such double twisted cylinders are impossible to tile the whole 3D space, which leads to inevitable disclinations and results in frustrated structures.

Self-organization is an intrinsic ability of LC molecules. However, the precise control and generation of large-area desirable hierarchical superstructures require state-of-the-art techniques that usually combine the “top-down” microfabrication with the “bottom-up” self-assembly. Here, we review various hierarchical architectures in SLCs, CLCs, and BPLCs, especially recent progresses in light-activated LC hierarchical superstructures, as well as their optics and photonics applications in optics and photonics. In this review, we will see the controllable spatial smectic layer curving via 2D anchoring confinement, 3D topographic confinement, and external field guidance, with which the domain size, shape, orientation, and lattice symmetry of focal conic domain (FCD) arrays are well manipulated. The control of helix direction or fluctuation of CLC layers and the growth of unique fingerprint textures including spiral and wave-like continuous gratings are presented. The 3D manipulation of BPLC hierarchical architecture is accomplished photoalignment and various light-driven azobenzene molecular motors. The construction of these unique hierarchical superstructures brings new opportunities to the design of novel optic and photonic devices. Corresponding applications, including traditional microlens array, beam steering, and more advanced specific optical field generation and LC lasers are comprehensively reviewed as well.

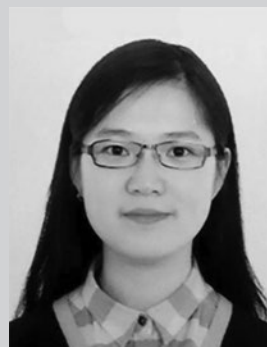
2. Light-Activated Liquid Crystalline Hierarchical Architectures

2.1. Smectic Layer Curvature Control

Among various soft materials, SLC, especially smectic-A (SmA) LC, has attracted much attention due to its distinct lamellar structure and reconfigurable smectic layer curvature.^[6a,10] Due to the energy constraint of preserving constant smectic layer thickness, splay deformations can be easily found in this phase when under antagonistic anchoring conditions.^[11] Consequently, periodic smectic layer curvatures are caused and resulting in a series of micron-sized defect structures.^[5a] The most common smectic layer deformations are modeled as families of the so-called “Dupin cyclides,”^[12] which are first discovered by Dupin. An implicit equation of Dupin cyclides is

$$(x^2 + y^2 + z^2 - \mu^2 + b^2)^2 - 4(ax - c\mu)^2 - 4b^2y^2 = 0 \quad (1)$$

where μ is a parameter that controls the shape of the Dupin cyclide; the numbers a , b , and c fulfill the conditions of $a > b > 0$, $c^2 = a^2 - b^2$, which determine the configuration of the ellipse

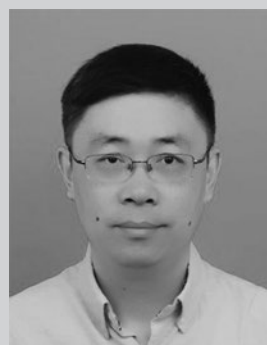


Ling-Ling Ma received her Ph.D. degree in optical engineering in 2019 from Nanjing University, China. She is currently at Nanjing University as a postdoctoral fellow with Professor Yan-Qing Lu and Professor Wei Hu. Her research is focused on the hierarchical architectures in self-assembled liquid crystals and the applications of liquid crystal superstructures.



Wei Hu is Tang Scholar and professor of optical engineering, Nanjing University, China. He earned his Ph.D. in polymer chemistry from Jilin University in 2009. His research fields are liquid crystal materials and optical devices, with a focus on photoalignment-enabled liquid crystalline hierarchical architecture, optically

addressed spatial light modulator, liquid crystal telecom, and terahertz elements. His initiative works on above topics have been widely recognized in materials, physics, and optics communities. He has published over 100 peer reviewed journal papers, 7 book chapters, and over 90 conference contributions, and holds 58 issued/pending patents.



Yan-Qing Lu received both his B.S. and Ph.D. degrees from Nanjing University, China, in 1991 and 1996, respectively. He has 5 year experiences in US and China telecom industries. He designed and developed a serial of liquid crystal-based fiber-optic devices with his colleagues, which include variable optical attenuators,

variable Mux/Demux, DWDM wavelength blocker, etc. He is currently a Changjiang distinguished professor at Nanjing University and a Fellow of Optical Society of America and Chinese Optical Society. His research interests include liquid crystal photonics, fiber optics, and nonlinear optics.

$$\frac{x^2}{a^2} + \frac{y^2}{b^2} = 1, \quad z = 0 \quad (2)$$

and the hyperbola

$$\frac{x^2}{c^2} - \frac{z^2}{b^2} = 1, \quad y = 0 \quad (3)$$

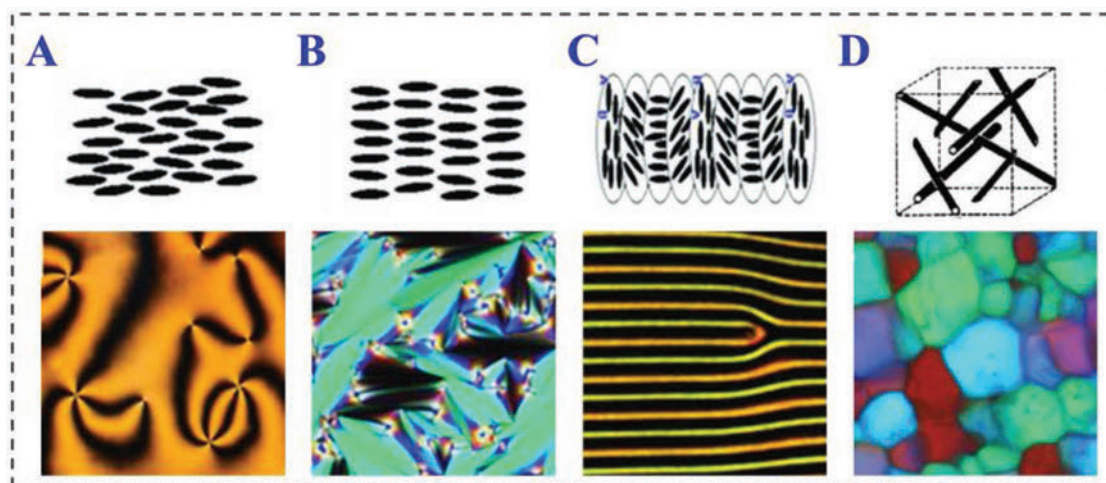


Figure 1. Four typical LC phases. A) Structure and schlieren texture of nematic phase LC, B) structure and focal conic texture of SLC, C) structure and fingerprint texture of CLC, D) double-twisted structure and mosaic-like platelet texture of BPLC. (A–C) Reproduced with permission.^[6a] Copyright 2011, Wiley-VCH. (D) Reproduced with permission.^[9] Copyright 2015, Royal Society of Chemistry.

Such cyclides are also known as “FCDs”. According to the Gaussian curvature of smectic layers in the Dupin cyclide

$$K = 1/(R_1 \cdot R_2) \quad (4)$$

which is defined by two principal radii of smectic layers R_1 and R_2 , FCDs can be divided into three different species: FCD-I, FCD-II, and FCD-III as shown in **Figure 2**.^[14] For FCD-I, the most typical defect structure existing in a thermotropic smectic phase, it has a negative K , ($R_1 \cdot R_2 < 0$). Within each FCD-I, parallel curved smectic layers wrap around a pair of conjugated defect lines, generally an ellipse and one branch of hyperbolae, which locate in two perpendicular planes and pass through each other's focal points.^[15] The FCD-II with an onion-like shape possesses a positive K . Whereas the smectic layers in FCD-III combine both positive and negative K as introduced by Kleman and Lavrentovich.^[15] Here in this report, we mainly focus on FCD-I with a negative K .

Nowadays, the topological defects in SLCs have been exploited for a wide range of applications, such as soft lithographic templates,^[16] superhydrophobic surfaces,^[17] microlens arrays,^[18] and particle assembly.^[19] It is a key requirement to have a precise control of the smectic layer curvature and generate different desirable topological superstructures. So far, much effort has been devoted to the 3D manipulation of smectic defects, including their sizes, shapes, orientations as well as the lattice symmetry, by referring to the boundary condition, film thickness, or applying external fields.^[6a] 2D anchoring or 3D geometric confinement carried out by photoalignment, photolithography, or other light-activated techniques has been well-recognized in the smectic layer curvature control. In addition, adopting external fields to dynamically vary the smectic layer configuration is intensively studied. These developments bring more fantastic soft materials with advanced functionalities.

2.1.1. 2D Anchoring Confinement

Surface anchoring induced by rubbed polyimide films plays key role in LC applications. Ok and co-workers introduced

multidirectional rubbing^[13] and multiple stamping^[20] methods to control the arrangement of toric FCDs (TFCDs). The TFCD is a well-studied topological defect mode in SLCs, where curved smectic layers wrap around two degenerated defect lines (a circle and a straight line), with the straight line passing through the center of the circle, causing a dimple-like defect shape.

As shown in **Figure 3A,B**, by changing the included angle between two successive rubbing directions or pressing a line-shaped stamp along two different directions, TFCD arrays with square, parallelogrammic, and hexagonal lattice symmetries were generated. It was found that the intersection of each two rubbing grooves and the stamping-introduced grid pattern could guide TFCDs assembling to an ordered array. And, the sizes of TFCDs could be tailored by simply changing the sample film thickness or the line intervals of the stamp. It is worth mentioning that the nematic-SmA phase transition is a key factor in both the controlling methods. Although these methods exhibit advantages of simplicity and wide industrial applications, disadvantages such as mechanical damage and electrostatic charge still could not be neglected.

To avoid the above problems, a dynamic light-activated photoalignment technique was adopted to control the 3D smectic layer curvature.^[21] **Figure 3C-I** schematically shows a digital mirror device-based photopatterning system,^[22] which can easily accomplish arbitrary planar anchoring patterns. By this means, hemi-toric FCDs with half-moon shapes were generated for the first time on a substrate with a periodically alternative $\pm 45^\circ$ alignment pattern (**Figure 3C-II**). Although defect lines of the hemi-toric FCDs were the same as TFCDs (**Figure 3C-III**), the other half structure was suppressed because of the violation of the underlying anchoring condition. The domain sizes of hemi-toric FCDs could be well controlled by changing the alignment period. Moreover, the domain orientations were also manipulated by altering the alignment directions of the periodic alignment pattern. By further introducing multidomain checkerboard photoalignment patterns, square lattices of different fan-shaped fragmented TFCDs were formed in **Figure 3C-IV**. Thus, it can be concluded that the 2D anchoring confinement

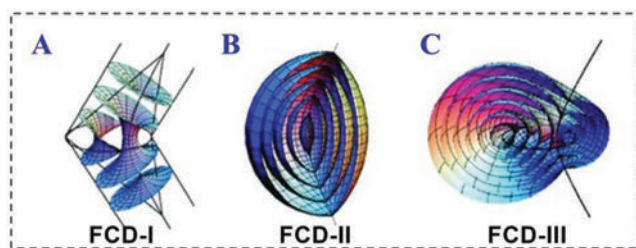


Figure 2. Three typical types of FCDs. A) Structure of FCD-I. The smectic layers are restricted to the negative Gaussian curvature parts. B) Structure of FCD-II with smectic layers of positive Gaussian curvature. C) Structure of FCD-III with both positive and negative Gaussian curvatures of smectic layers. Reproduced with permission.^[15] Copyright 2009, Taylor & Francis.

(including both the alignment direction and pattern) is able to effectively guide the smectic layer curvature and simultaneously control the size, shape, orientation, and arrangement of smectic defects. It verifies the feasibility of light-activated smectic layer origami, which may open up a door toward the creation of more fantastic lamellar hierarchical superstructures.

2.1.2. 3D Topographic Confinement

Besides the 2D anchoring confinement, Yoon and co-workers reported ordered TFCDs confined by photolithographic microchannels (Figure 4A) and directly visualized the internal smectic layer curvature within each TFCD.^[19] In addition to the 3D topographic confinement, the internal surface alignment of the microchannels and the SLC molecular structure were also key parameters that would determine the long-range-ordered TFCD array. For example, Shin et al. produced various periodic arrays of topological defects, including tilted FCDs with nonzero

eccentricities and zigzag patterns by presetting anchoring conditions of the microchannels.^[23] And, SLC materials with fluorinated moieties would facilitate the generation of highly ordered TFCD arrays compared to those with alkyl chains. The reason might be attributed to the electronegative property, which made the smectic layered structure more stable.^[24]

The shape of the microchannel plays a crucial role in smectic layer curvature as well. Kim et al. varied the cross-section shapes of microchannels to better regulate the TFCD arrays with alkyl-terminated SLC material, like 8CB.^[25] These microchannels were fabricated on (100) Si wafers by a photolithography technique. Planar alignment was designedly introduced to inner surfaces of the channel to provide an antagonistic anchoring condition for SLCs. As shown in Figure 4B, it was found that among different shaped microchannels, only those with trapezoidal cross-section shapes could form highly monodispersed periodic TFCDs. This phenomenon was mainly attributed to the inclined side walls and flat bottom space of the trapezoidal channel compared to the rectangular and V-shaped microchannels. It was the combining effect of the anchoring and the side wall directing that resulted in the special formation of TFCD structure. Moreover, the sizes and arrangement of TFCDs could be also controlled by varying featured dimensions of the bottom width and depth of trapezoidal microchannels.

Micropillars supply another 3D topographic confinement way for smectic layer curvature control. In ref. [26], the authors systematically studied the role of micropillar-patterned substrate in producing ordered TFCD arrays. The domain size and lattice symmetry of the TFCD array were highly dependent on the geometry (size, height, and spacing) and lattice symmetry of the cylindrical micropillar array. Notably, to form a TFCD array on a flat substrate, a certain film thickness ($\geq 2 \mu\text{m}$) is required.^[27] Thus, for a given substrate with micropillars, the growing of TFCDs between neighboring pillars or on the top

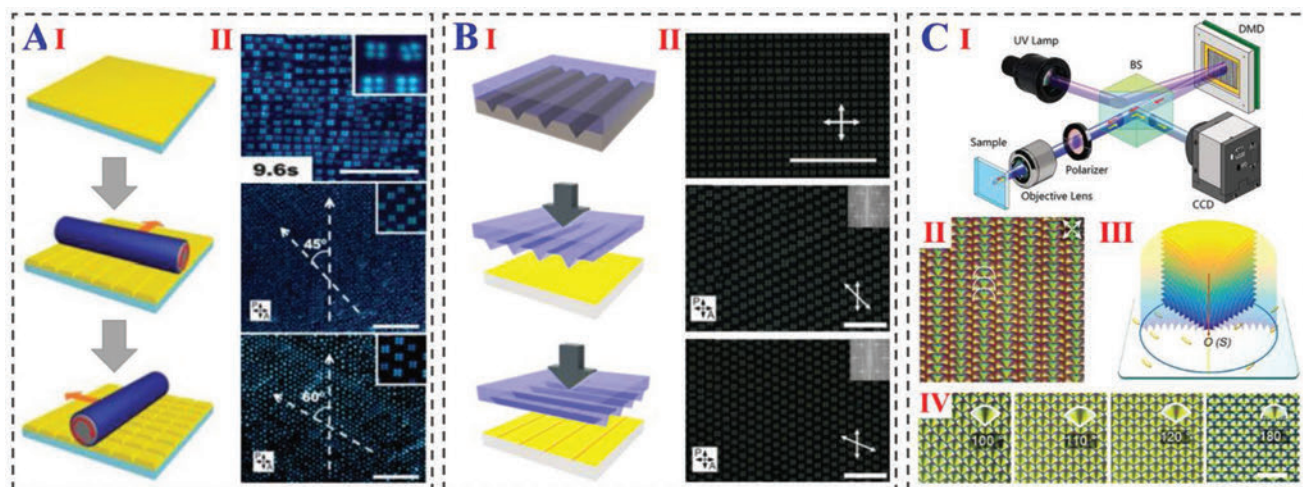


Figure 3. Smectic layer curvature control via LC alignment techniques. A, B) Multidirectional rubbing and multiple-stamping domain separation methods. I) Schematic illustration of the fabrication processes. II) Polarized optical microscopy (POM) images of the TFCD arrays with square, parallelogrammic, and hexagonal arrangements. The scale bars in (A) are $50 \mu\text{m}$. The scale bars in (B) are $100 \mu\text{m}$. C) Photoalignment method. I) Schematic illustration of the digital micro-mirror device-based photolithography setup. II) POM texture of the hemi-toric FCD array. III) 3D model of the hemi-toric FCD. IV) Differently fan-shaped FCD arrays generated on multidomain checkerboard photopatterned substrates with different anchoring orientations. The scale bar is $20 \mu\text{m}$. (A) Reproduced with permission.^[13] Copyright 2011, Royal Society of Chemistry. (B) Reproduced with permission.^[20] Copyright 2016, American Chemical Society. (C) Reproduced with permission.^[21] Copyright 2017, Wiley-VCH.

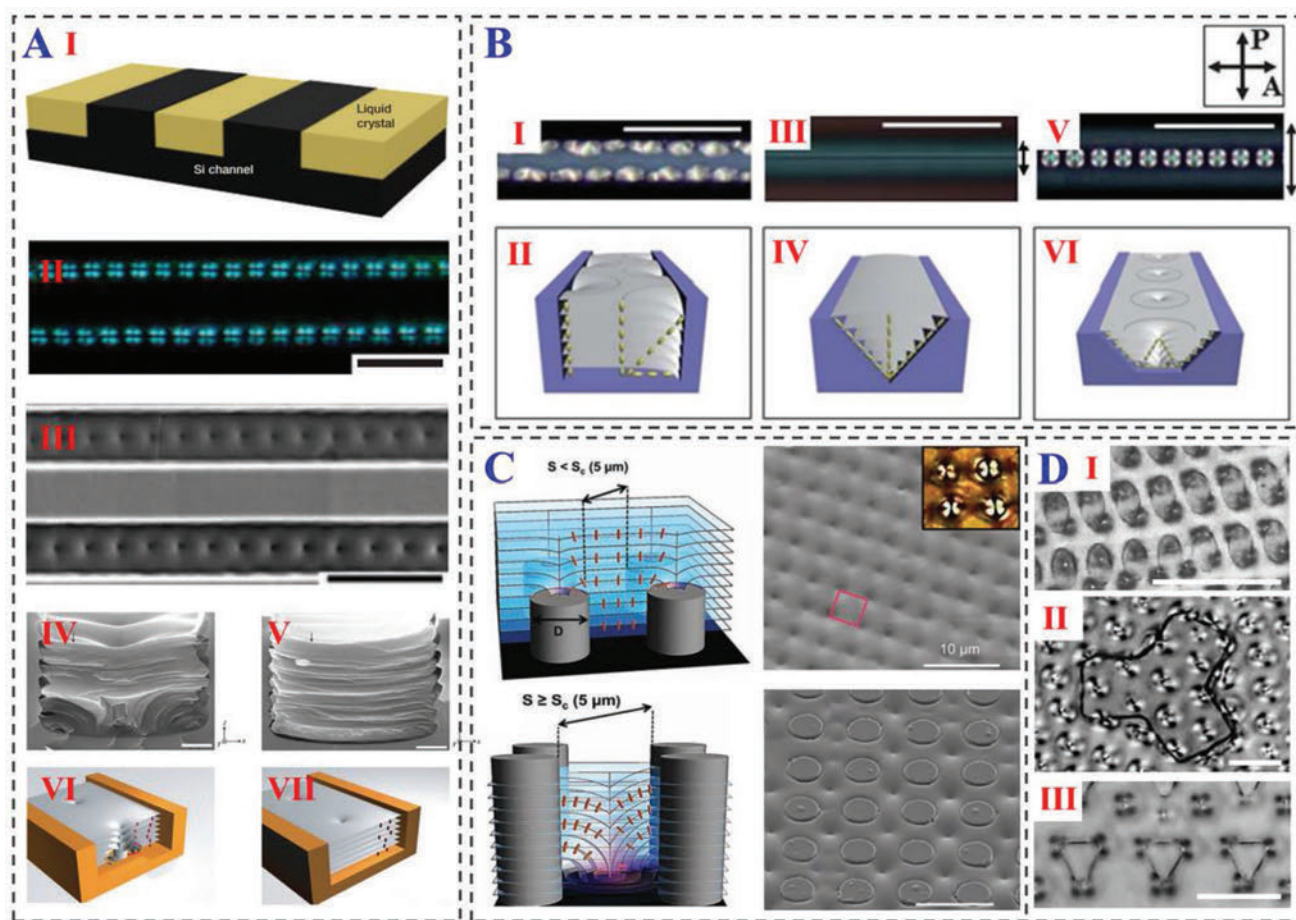


Figure 4. Smectic layer curvature control based on 3D topographic confinement. A) Rectangular microchannel confinement and a direct visualization of the smectic layer configuration within a TFCD. The scale bars in (II and III) are 10 μm ; the scale bars in (IV and V) are 1 μm . B) Microchannel confinement with I,II) rectangular, III,IV) V-shaped, and V,VI) trapezoidal channel shapes. The scale bars are 50 μm . C) Cylindrical micropillar confinement. D) Micropillar confinement with I) elliptically, II) “Y”, and III) triangularly pillar shapes. The scale bars are 20 μm . (A) Reproduced with permission.^[19] Copyright 2007, Nature Publishing Group. (B) Reproduced with permission.^[25] Copyright 2011, The Royal Society of Chemistry. (C) Reproduced with permission.^[26] Copyright 2011, Wiley-VCH. (D) Reproduced with permission.^[6c] Copyright 2013, National Academy of Sciences USA.

of each pillar also depended on the sample film thickness (Figure 4C). Furthermore, they changed the micropillar shape to realize more fantastic FCD arrangements by pinning smectic defects on edges of the micropillars (Figure 4D).^[6c] With this method, the geometry of micropillars should be optimized for desired domain size. In addition, the eccentricity of resultant FCDs were able to be tuned by changing the size and spacing of the pillar array. Both the 2D anchoring confinement and 3D topographic confinement have their own superiority, and the latter makes more complicated operation available, although it is sophisticated.

2.1.3. External Field Control

Thanks to the intrinsic sensitivity of LCs to various external stimuli, the smectic layer curvature can be controlled via external fields as well, such as electric field^[28] and thermal field.^[5b,6b,29] For example, Gim and Yoon introduced an in-plane electric field (≈ 30 V, 1 kHz, Figure 5A) to the TFCD

array within microchannels, and found that columns of toric defects (Figure 5B) were transformed to a periodic zigzag pattern (Figure 5C).^[28a] Further increasing the electric field to ≈ 100 V, the LC molecules were forced to reorient parallel to the electric field (Figure 5D). These phenomena suggest that the smectic layer configuration can be dynamically controlled by electric field. To keep focusing on the scope, we will not go for further details on the smectic layer curvature control with other external fields.

2.2. CLC Helical Superstructure Manipulation

Cholesteric phase is endowed with an intrinsic self-organized helical structure with a well-defined periodicity and handedness. Such structure is derived from the inherent chirality of cholesteric molecules or the participation of additional chiral dopants in achiral nematic LCs. Helical pitch (p), defined as the length of one turn of the LC director rotation along the helical axis, roughly ranges from a hundred nanometers to several

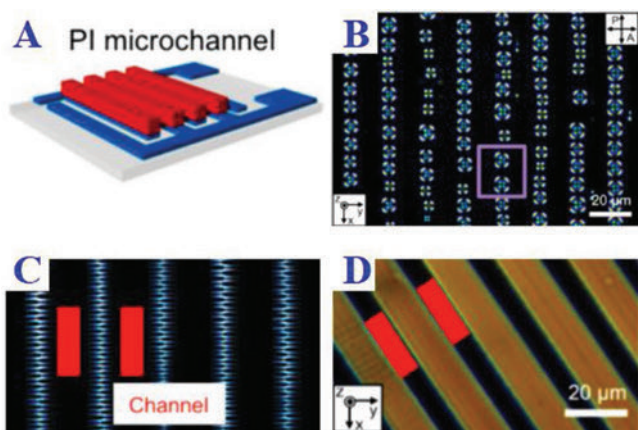


Figure 5. Smectic layer curvature control with an in-plane electric field. A) Schematic illustration of the polyimide microchannels on patterned indium tin oxide electrodes. B–D) POM textures of TFCDs (0 V), zigzag patterns (30 V, 1 kHz), and vertically aligned smectic lamellar structure (100 V, 1 kHz). The scale bars are 20 μm . Reproduced with permission.^[28a] Copyright 2016, American Chemical Society.

micrometers and is determined by $P = 1/(\text{HTP} \cdot c\%)$, where HTP denotes the helical twisting power and $c\%$ represents the weight ratio of the chiral dopant in CLC. Depending on the anchoring condition, CLCs exhibit distinct textures with different helical structures. For instance, when in a homogeneously planar cell,^[30] CLCs self-organize into a standing helix (SH) structure with all helical axes perpendicular to the substrates, presenting a planar texture. Such structure possesses an attractive property of selective reflection for circularly polarized light. For a cell with homeotropic alignment,^[31] lying helix (LH) structure occurs as shown in Figure 1C with helical axes parallel to the substrate surfaces. Due to the lack of specific helix orientation, the LH structure usually shows a texture resembling our fingerprints, hence named “fingerprint texture.” When CLCs are confined within a hybrid alignment cell (the two substrates are treated with unidirectional planar and homeotropic alignments, respectively) or coated on a single substrate with a homogenous alignment boundary condition,^[32] the helical layers adjacent to the homogeneously aligned substrate maintain a planar state, while CLC layers near the LC/air interface experience a periodic distortion.

Thanks to the aforementioned unique helical structures, CLCs have been widely studied so far and numerous fancy applications based on CLCs have been exploited, such as sensors,^[33] displays,^[34] lasing,^[35] smart windows,^[36] beam steering,^[37] flexoelectro-optic devices as well as various optical elements.^[38] Whereas all these practical applications need excellent control of the hierarchical architectures in CLCs. Hence, except for the boundary condition, external stimuli are also favorable in tuning the helical pitch, multidimensional, and dynamic control of the CLC helix. For example, when applying a proper electric field, the helical structure will be transformed from an SH mode to an LH mode in a homogeneously aligned cell.^[39] Light field, as a facile stimulus, has its own prominent advantages compared to other external field, e.g., noncontact remote control, unconstrained on the requirement of materials and avoiding complicated structural design of devices. In the following, we mainly focus on the light-activated helical superstructure manipulation (including

photopatterning and light-driven CLCs) and present dynamic helical structure controls (such as in-plane rotation of lying helical axes^[40] and inversion of the helical handedness^[41]).

2.2.1. Photoalignment and Photopatterning of CLCs

Traditional mechanical rubbing techniques have been extensively used in LC alignment. Recently, photoalignment techniques based on photoresponsive agents have been proposed as a more promising mean in high-quality LC alignments.^[22a,42] Compared to the mechanical rubbing technique, photoalignment techniques avoid any mechanical damage, electrostatic charge, and dust contamination and has clear superiority in complex multidomain alignments of LCs. Thanks to its feasibility of aligning diversiform LC materials, Ma et al. employed a dynamic photoalignment technique based on a polarization-sensitive sulfonic azo dye SD1 to rationally design and arbitrarily control the in-plane helical axes of CLCs (Figure 6A).^[39a] Moreover, they were able to do this over a scale of several centimeters. With the aid of electric field, the SH and LH states could be reversibly switched between each other. As the capability of CLC helical structure manipulation was significantly extended, unique fingerprint textures, including Archimedean spiral and wave-like continuous gratings are achieved easily. Moreover, general rules behind the helical axis manipulation were also investigated. This work verifies the feasibility of CLC helical superstructure manipulation via photoalignment and will bring in new superstructures with exceptional features for more advanced functional devices.

Methyl red (MR)-doped LCs are also known as a light-activated bulk-mediated alignment method.^[40a,43] Under the irradiation of polarized green light, the azo dye molecules dissolved in the LC host will undergo absorption, photo-isomerization, diffusion, desorption, and then adsorb to the substrates. The MR dyes reorient adjacent LC molecules to form a unidirectional alignment. Li et al. presented an asymmetric photoalignment approach to modulate the fingerprint textures of MR-doped CLC in a cell with one substrate untreated and the other coated with uniformly rubbed polyimide layer (Figure 6B-I).^[40a] The light-activated multivariant control of the stripe directions of fingerprint textures is presented in Figure 6B-II–V with the aid of a proper electric field. More sophisticated periodic CLC gratings in the shapes of dashed curves and dashed lines were also demonstrated by one-step polarization holography of two orthogonal polarized beams. It is believed that photopatterning of CLCs will definitely enrich the research contents of controllable hierarchical architectures in soft LC building blocks.

2.2.2. Light-Driven Photoresponsive CLCs

Another light-activated CLC helical superstructure tuning is enabled by introducing photosensitive chiral dopants into the material systems.^[44] Under the irradiation of suitable light, such dopants usually experience a photoinduced isomerization, acting as molecular motors or switches and thus adjusting the HTP. Compared with electrical and magnetic manipulation,^[39b,45] light control will provide higher spatial and temporal precision and possesses remote and digital controllability.

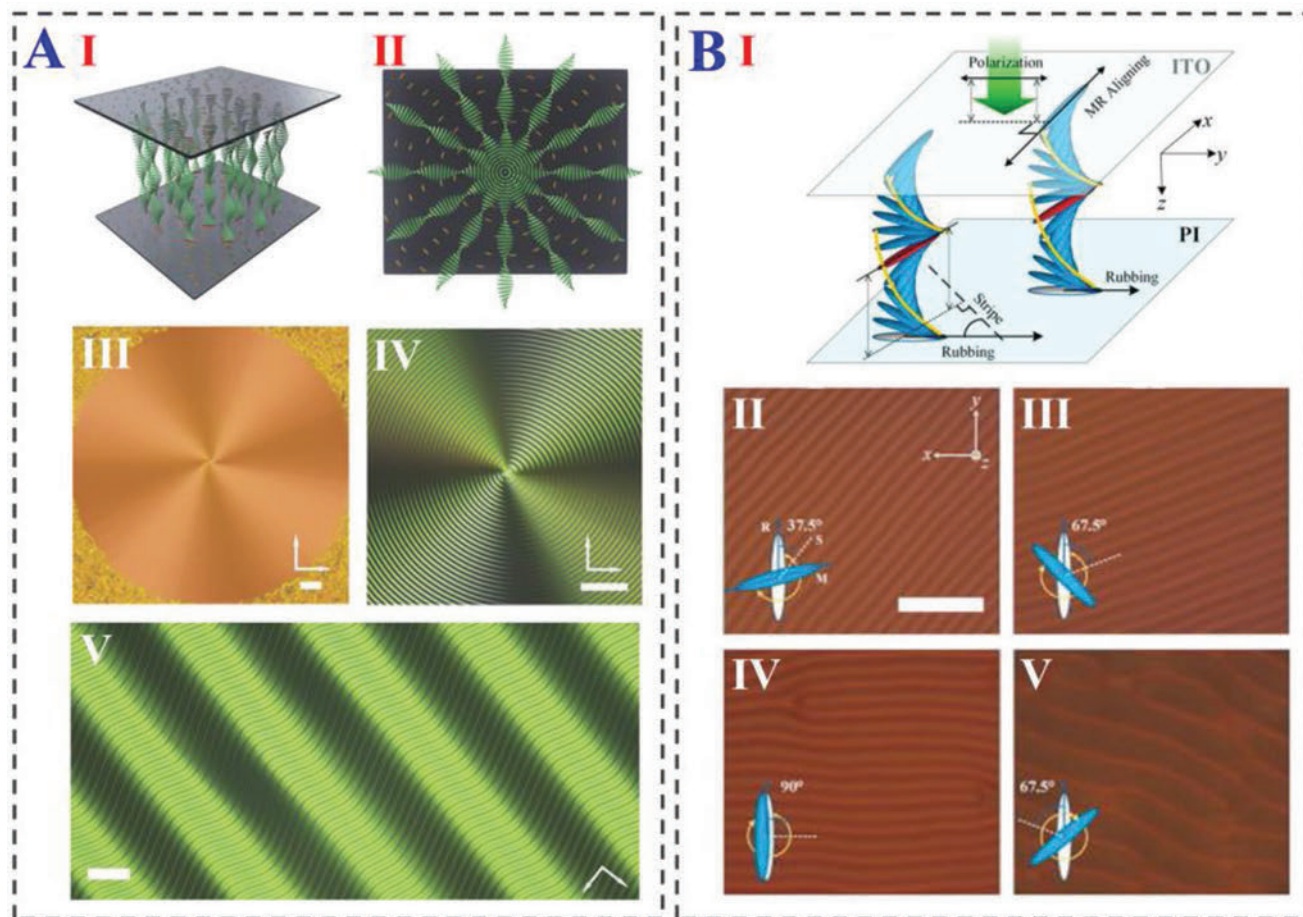


Figure 6. CLC helical structure manipulation via photopatterning. A) Photopatterning based on a dynamic photoalignment technique with SD1. I,II) Schematic diagrams and III,IV) POM images of circularly aligned CLCs in SH and electric field-induced LH states. The scale bars are 50 μm . V) POM image of a wave-like CLC grating. The scale bar is 20 μm . B) Photopatterning based on an MR-doped CLC material system. I) Configuration of the photoalignment process. II–V) POM images of varied periodic fingerprint textures. The scale bar is 50 μm . (A) Reproduced with permission.^[39a] Copyright 2015, Wiley-VCH. (B) Reproduced with permission.^[40a] Copyright 2017, American Institute of Physics.

Recently, CLC gratings formed in semi-free films have attracted intensive attention.^[46] Ma et al. reported light-driven CLC gratings fabricated by spin-coating photosensitive CLCs onto a single substrate with a unidirectional planar photoalignment.^[47] In this situation, the LC/air interface provided with a near-vertical alignment. Accordingly, planar helical layers existed near the substrate while periodically distorted layers were formed adjacent to the opposite interface (Figure 7A-I). Then the authors systematically investigated the light-activated continuous rotation and pitch-tuning behaviors of the CLC gratings, from which several useful rules were extracted and the maximum rotational angle of 987.8° was reached (Figure 7A-II,III). Thanks to the opening characteristic of the material system, precise beam steering and synchronous micromanipulation were also demonstrated (Figure 7A-IV). This work extends the understanding of semi-free soft mater systems and supplies new opportunities for novel applications-based light-activated CLC gratings in semi-free systems.

Elkema et al. synthesized a special light-driven molecular motor (Figure 7B-I) and demonstrated a reversible handedness inversion of the CLC helical structure due to the photochemical

isomerization.^[41a] Upon UV light irradiation, the resultant fingerprint texture exhibited a clockwise rotation, accompanied with a helical pitch change. And the anticlockwise rotation emerged due to the dark thermal relaxation after removing the light source. As shown in Figure 7B-II, such light-activated CLC structures could be used in rotational controls of microparticles, which may provide a bright future for nanomachines with molecular-scale motors.

For other dimension control of the CLC helical superstructure, Zheng and co-workers introduced an axially chiral molecular switch (*S,S*)-D4 (Figure 7C-I) to a CLC system and realized both the 3D manipulation and an handedness inversion of the CLC helix stimulated by a facile light.^[41b] Upon UV irradiation (310 nm), the photochromic dopants were transformed from a ring-open structure to a ring-closed isomer, resulting in the handedness inversion (from the initial right-handed to the left-handed form). Accordingly, the helical superstructure was transformed from the SH state to the uniform LH state, followed by an in-plane rotation of the helical axes (Figure 7C-II). In addition, the reverse process occurred when the sample was exposed to visible light (550 nm).

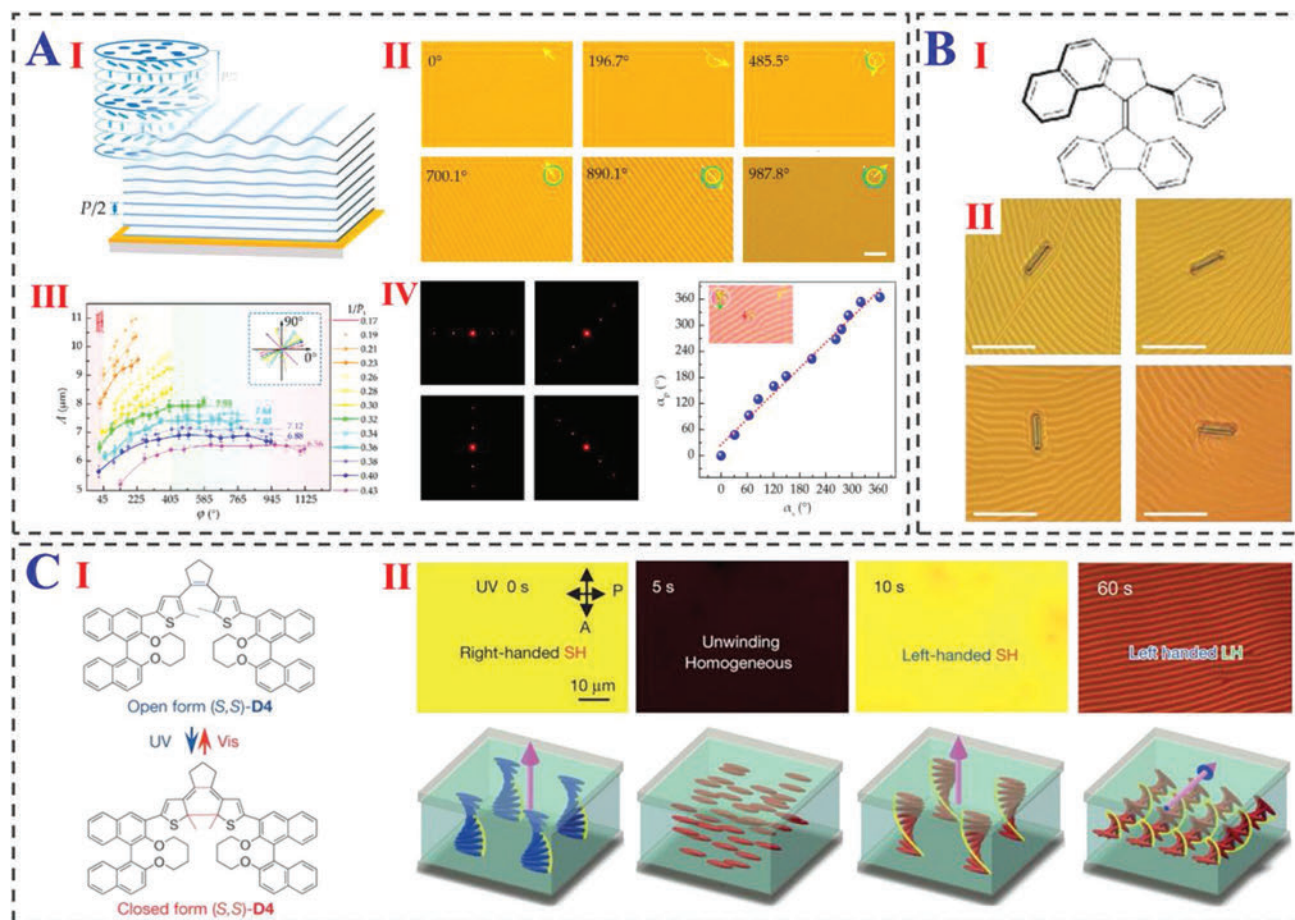


Figure 7. Light-driven CLCs based on photosensitive chiral molecular motors and switches. A) Light-driven rotation and pitch-tuning of the CLC grating in a semi-free film. I) Schematic diagram of the deformed helical structure in a CLC grating. II) Light-activated CLC grating rotation. III) Dependencies of the grating period and orientation on the concentration of chiral dopant and the exposure dose. The scale bar is 25 μm . B) Rotational CLC grating based on a photochromic molecular motor. I) Molecular structure of the nanomotor. II) Rotational behaviors of the CLC grating and a microscale object during irradiation with ultraviolet light. The scale bars are 50 μm . C) Light-induced 3D control over the CLC helical axes. I) Molecular structure of the chiral molecular switch, (S,S)-D4, and diagram of its phototransformation process. II) Transformation process of the helical superstructure in a unidirectional planar cell under UV irradiation (from the right-handed SH state, unwinding homogenous state, left-handed SH state to the left-handed LH state). (A) Reproduced with permission.^[47] Copyright 2017, MDPI. (B) Reproduced with permission.^[41a] Copyright 2006, Nature Publishing Group. (C) Reproduced with permission.^[41b] Copyright 2017, Nature Publishing Group.

The light-activated multidimensional control over the helical axes of CLCs advances the realization of complex smart systems and reconfigurable 3D architectures.

2.3. Light-Activated BP 3D Soft Lattice

BP is generally divided into three types of sub-phases determined by the distribution of phase disclination lines, i.e., the amorphous BPIII with disordered distributed disclination lines, the cubic BPII and BPI with disclination lines like the scaffolds of the 3D lattices. Optically, for one thing, BPIII displays a fluid fog-like texture, while BPII and BPI present a similar gorgeous colorful mosaic-like platelet texture caused by the Bragg selective reflection of the lattice, although their topological structures of the lattices are completely different, i.e., the former has a simple cubic lattice and the latter owns a body centered

cubic lattice. For another, BP is optically isotropic, resulted from the statistically homogenous direction of LC molecules, which enables sufficient prospective applications on the next-generation displays,^[48] photonics,^[49] and others beyond.^[50] So far, BP has attracted accumulative attentions toward both the fundamental sciences and the application engineering.

Although the conspicuous progresses of BP in the past several years, ranging from materials,^[48,51] optics,^[49] and devices,^[48,52] suggest its incremental developments and brilliant futures, the research of light-activated BP, however, evolves slowly as a mutually concerned scientific issue.^[53] Actually, BP superstructures driven by a facile light stimulation are more preferable on account of its aforementioned superiority. As aforementioned, such a fantastic photoresponse function is generally realized by judiciously functionalizing the common BPLC with photochromic groups, for instance, the azobenzene. The original BP arrangement suffers a deformation owing

to the combination effects of the photoisomerization of the photochromics and the long-range order of LC molecules, thus attaining the manipulation of BP lattice solely by light.

2.3.1. Photoresponsive BPLC Enabled by Azobenzene Derivatives

The photoresponsive behaviors of BP were systematically investigated from the perspective of spectroscopy for the first time in a system containing the azobenzene-functionalized photosensitive nematic LCs and the common photo-insensitive chiral agent.^[54] After a proper exposure dose of UV light, both the peak wavelength and the bandwidth (i.e., full-width at half-maximum) of the selective reflection spectra were changed. This phenomenon was caused by the LC molecular geometry change (from a linear *trans*-isomer to a bent-shaped *cis*-isomer), which led to a decrease of optical anisotropy of LCs, a weakening of orientation orderliness as well as a compression of the lattice constant of BP arrangement. Therefore, the reflection

band exhibited a blue-shift accompanied by a narrowing of the corresponding band-gap in accordance with the relationship

$$\lambda_p = \frac{2\langle n \rangle a}{\sqrt{h^2 + k^2 + l^2}} \quad (5)$$

Herein, λ_p is the peak wavelength, a is lattice constant which is determined by the helical pitch and lattice arrangement, $\langle n \rangle$ denotes the average refractive index, while h, k, l are Miller indices of BP lattice. More specifically, the phase transition from BPI to BPII and even an induction of BP in a cholesteric system were observed, which were attributed to the chirality enhancement of the system after a certain dose of UV irradiation.

Such a groundwork inspired another intriguing strategy by homogeneously mixing a commercial photoinactive nematic LCs with a photoactive azobenzene derivative. **Figure 8A-I** presents the rod-like molecular structure of the azobenzene derivative, which is similar to that of common nematic LCs.^[55] A typical BP optical texture, reflecting a reddish yellow color with the

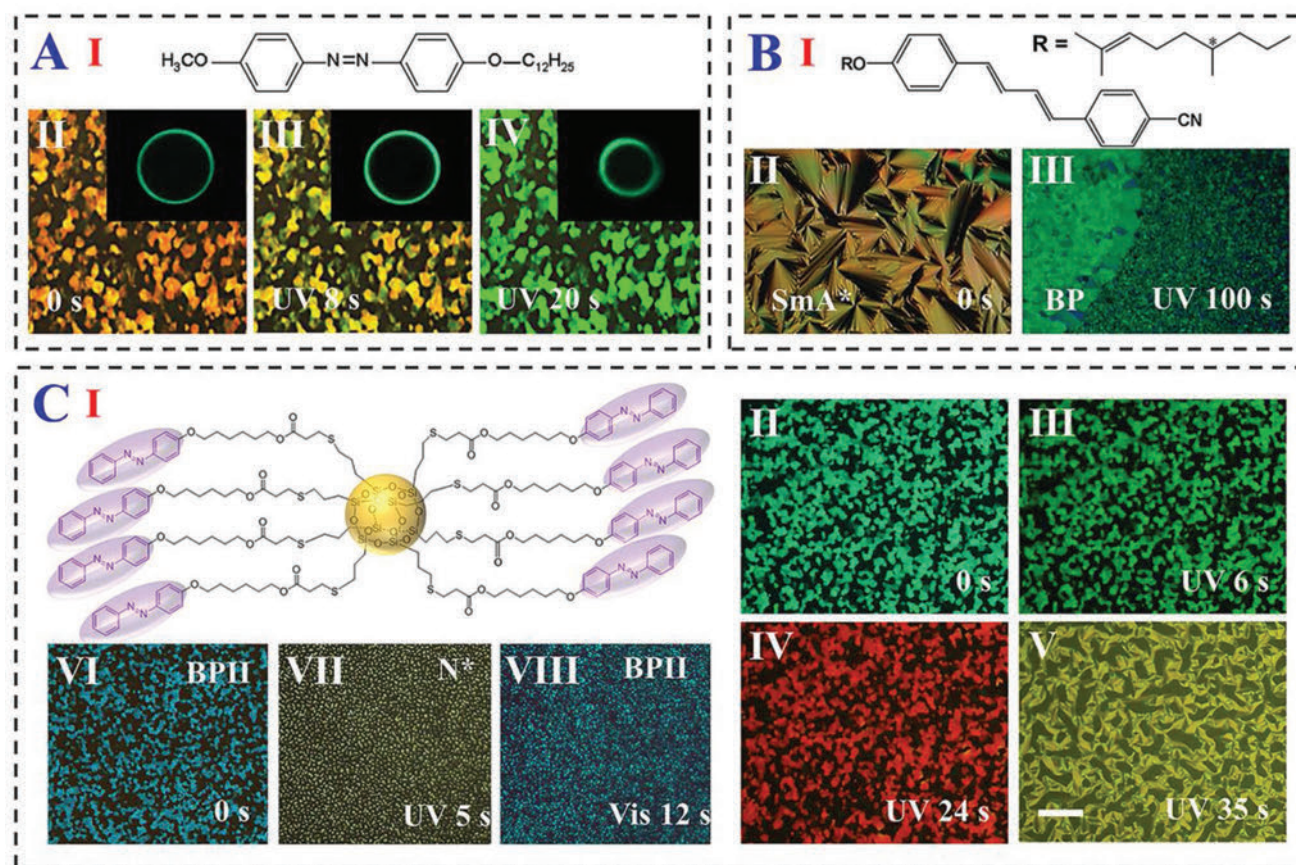


Figure 8. Photoresponsive BP based on the rod-like photosensitive molecules and moieties. A) Light-induced blue-shift of reflection color (II–IV) of the BP containing rod-like azobenzene (I). The insets of (II–IV) are the Kössel diagrams of the corresponding textures. B) The chiral smectic A (SmA*) LCs (II) with a diphenylbutadiene structure (I) transits to BP (III) with a UV exposure for 100 s. C) A photoresponsive simple cubic BP (II) can be induced by a POSS nanocage functionalized by photosensitive mesogenic azobenzene moieties, Azo-POSS (I). The reflection color changed from the initial cyan color, passing through green (III) to red (IV) when the sample is irradiated by UV light. Further irradiation induces a phase transition BP to chiral nematic phase (V). The simple cubic BP transits to chiral nematic phase after suffering a 5 s UV exposure, and the similar simple cubic BP can be reconfigured by a further exposure with 532 nm visible light for 12 s (VI–VIII). The scale bar is 100 μm . (A) Reproduced with permission.^[55] Copyright 2010, American Institute of Physics. (B) Reproduced with permission.^[57] Copyright 2010, Royal Society of Chemistry. (C) Reproduced with permission.^[58] Copyright 2018, Wiley-VCH.

corresponding peak wavelength at 610 nm, existed in a temperature range from 27.1 to 43.6 °C. Its reflection spectrum blue-shifted for about 60 nm and the reflective color changed from the reddish, yellow, yellowish green to the green color within 20 s during the continuous irradiation of blue light (Figure 8A); while the recovery was implemented by switching the blue light to a green one. The lattice deformation was further corroborated through the Kössel diffraction,^[56] which was a convincing methodology to reflect the orientation and deformation of a cubic structure, under an impinging of cone laser with the light wavelength matching the lattice constant. The circular ring Kössel diagram and the shrinkage of its diameter indicated a (2, 0, 0) lattice orientation and an expanding of the lattice during the blue-light stimulation.

Moreover, a stable BP (Figure 8B-III) based on photoresponsive diphenylbutadiene mesogenic molecules containing a chiral carbon (Figure 8B-I) was achieved by UV light exposure.^[57] An ingenious design of a polyhedral oligomeric silsesquioxane (POSS) nanocage functionalized by photosensitive mesogenic azobenzene moieties (Figure 8C-I) was synthesized and homogeneously mixed into the chiral LCs.^[58] Herein, a fantastic aspect needing to be referred is that a photoresponsive and stable BP II simple cubic lattice (Figure 8C-II-V) achieved in such system,

which was confirmed through the aforementioned Kössel diffraction technique, is uncommonly existed in soft condensed matter. Furthermore, such a simple cubic BP collapsed during the UV exposure and recovered with a subsequent light irradiation with visible light (Figure 8C-VI-VIII), realizing a stable and reconfigurable simple cubic soft lattice solely by light.

Very recently, a kind of photoresponsive chiral molecular switch based on an axially chiral binaphthalene decorated with two photosensitive mesogenic azobenzenes was judiciously synthesized and mixed into a common LC material to generate a light-activated CLC, which presented both diverse phase transition behaviors and an extremely wide modulation range of P.^[6a,10] Such predominated attributes were precisely transplanted into the BPLC with a delicately designed concentration to enhance the light controllability. As shown in Figure 9A-II, a dynamic and reversible optically tunability of the BP reflection band,^[59] covering red, green, and blue, i.e., the three primary colors, was impressively manifested, which would be an ingenious contribution with sufficient application significances in the next-generation colorful displays and illuminations. A noteworthy aspect herein, which was entirely distinct with the aforementioned results, was a light-induced phase transition from the initial BP II to BPI caused by the significant weakening on

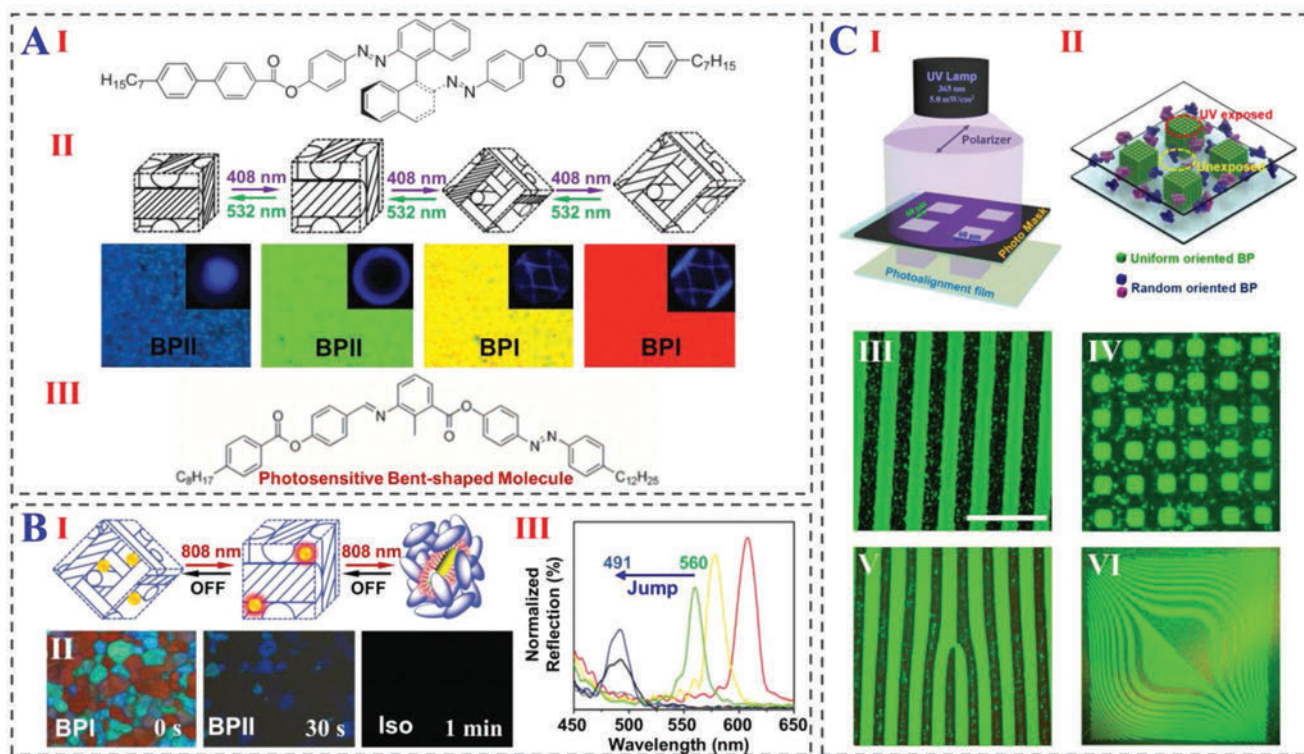


Figure 9. Light reconfigurable BPs based on other specific photosensitive materials. A) Light manipulated red, green, and blue reflection color of BP (I) enabled by an azobenzene-grafted binaphthalene (I). A designed bent-shaped azobenzene photosensitive material (III) to induce a BP with a light irradiation. Insets in panel II are the Kössel diagrams of the corresponding textures. B) NIR photoresponsive BP achieved by a prescribed gold nanorod with an absorption at NIR band. The schematic diagram (I), optical textures (II), and the corresponding reflection spectra, showing a jump of reflection wavelength from 560 to 491 nm (III), during the exposure of NIR light (808 nm) for 1 min. C) Photoalignment film-controlled lattice orientation of BPs and the micropatterning through photomask. The schematic diagram of the mechanism (I,II) and the generated micropatterns (III-VI). The scale bar is 300 μm. (A-I,II) Reproduced with permission.^[59] Copyright 2013, Wiley-VCH. (A-III) Reproduced with permission.^[62] Copyright 2012, Royal Society of Chemistry. (B) Reproduced with permission.^[9] Copyright 2015, Royal Society of Chemistry. (C) Reproduced with permission.^[63] Copyright 2017, Wiley-VCH.

the chirality of the system during an irradiation with short-wavelength light source. Such phase transition also led to a discontinuous shift of reflection band due to the variation of lattice orientation, i.e., there existed a spectral jump from the peak wavelength of 520–560 nm during the irradiation with 408 nm light.

A further investigation utilized a similar azobenzene-grafted binaphthalene photoresponsive chiral agent but decorated as a proton acceptor, while the octanoic acid was selected as the proton donor, thus forming hydrogen-bond complexes in chiral LCs.^[60] Such hydrogen-bonded chiral azobenzene switches played a positive role to generate a more stable BPI phase with a reversible spectral modulation in the range from 473 to 642 nm. Since there was no phase transition in this process, the shift of reflection spectrum was also continuous. A subsequent study, focusing on the molecular design of the azobenzene-grafted binaphthalene chiral molecular switch, found a remarkable performance on the helical twisting power. This study also indicated that the light tuning rate of BPLC was dependent on the grafted position of azobenzene on binaphthalene.^[61] Moreover, BPLC containing such kind of ingenious chiral molecular switch was refilled into a polymer film, which acted as a BP template recording a prescribed BP structure with an opposite-chirality of double twisted cylinders, to design and achieve new structures with unique features.^[50b] An intriguing example is a polarization-independent BP reflector, i.e., both the right-circular and left-circular polarized lights can be reflected, possessing photoswitchable reflection band as well.

Structure stabilization of BP is always a paramount aspect whatever in device elements or systems.^[64] Bent-shaped molecules, also known as “bent-cores,” have particular biaxiality owing to the bent molecular geometry, which has been confirmed to be efficient on enhancing BP stability.^[65] Therefore, another kind of photosensitive azobenzene-based bent-shaped materials (Figure 9A-III) was synthesized and embedded into the chiral LCs to explore the phase transition behavior during light exposure.^[62] Surprisingly, a cubic BP texture was induced in a chiral LCs (without BP) by suffering a UV light irradiation for about 20 min. Such induction was probably caused by the photoisomerization-induced reduction of orientation order of LCs, which compelled the *cis*-isomer of the photosensitive component to remain in the disclination lines of BP and thus stabilized BP. More importantly, such a stable BP can be maintained for a relatively long time after ceasing the UV light irradiation, resulted from the bent molecular geometry of bent-shaped molecules.

Considering from the other aspect, the isomerization of the bent-core molecule from a *trans*-conformer to a *cis*-one inevitably alters its molecular biaxiality, which probably influences the phase transition behavior of a chiral LCs, i.e., the bent molecular geometry is benefitted for generating a BP arrangement, while the linear geometry is adverse. Two kinds of azobenzene-based materials,^[66] with linear and bent *trans*-isomer, respectively, were mixed into the chiral LCs host after undergoing an elaborate conceiving. Therefore, two completely different phase transition phenomena were presented, a transition from cholesteric phase to BP for the system doped with the former materials^[66a] and a reverse transition with respect to the system doped with the latter material.^[66b] The aforementioned results further

confirmed the positive effect of bent-shaped molecules on the generation and stabilization of BP.

Furthermore, in the very recent, a similar azobenzene-based bent-shaped molecule with two azo moieties was adopted to comprise the photoresponsive BPLC.^[67] What inspired a great research enthusiasm was the selective stabilization, depending on the geometry of such photochromic molecule, i.e., the *trans*-isomer with a “V” shape was apt to stabilize the BPI phase, while its *cis*-isomer with a “W” shape was preferred to stabilize BPII phase. The reason of such an amazing distinction is closely related to the relative reduction of orientation order of LCs after suffering the photoisomerization, and further decreased the cost of splay and bend elastic energies for maintaining the BP cubic architecture.

2.3.2. Light-Activated BPLC via Photothermal Effect and Photoalignment

It is worth paying an extensive attention that another advanced materials and technologies have been utilized for equipping photoresponse of BPLC aside from the doping of photosensitive organic additive. The most representative ways are loading nanoparticle in BPLC and controlling molecular alignment on the surface of cell substrates. Nanoparticles with specific optical features have been one of a vital field in nanoscience and smoothly tried to integrate into soft materials so far, such as the light-induced illumination core-shell nanoparticle used as a transducer to convert a long-wavelength light to a short-wavelength one, thus achieving a photoresponsive CLC using near-infrared (NIR) light.^[68] In addition, the photothermal effect of the metallic nanoparticle and carbon nanomaterials, caused by light absorption after the material was irradiated by a light with certain wavelength closing the maximum of absorbance, was properly dispersed into the LCs to modulate the phase transition behaviors.^[69]

The aforementioned photoresponsive BPLC was stimulated by UV and visible (recovered process) lights, however in some specific situations, a low-energy and low damage threshold NIR light used as a driving source is more preferable.^[9] For the purpose of achieving an NIR-sensitive BPLC, the gold nanorods with a prescribed peak position of absorption was elaborately designed in accordance with an empirical equation, $\lambda_{\text{max}} = 95\eta + 420$, wherein, λ_{max} is the peak wavelength of the corresponding absorption spectrum, while η denotes the aspect ratio of such nanorods. The surface of gold nanorods was functionalized by a surfactant having an LC-like geometry to enhance the dispersion in LCs (Figure 9B-I). A 808 nm laser with the intensity of 2 W cm^{-2} was selected as the driven source, the reflection color of such gold nanorod-loaded BPLC altered from the initial red, passing through green, and finally reached blue, thus realizing an NIR-manipulated R, G, B reflection with less than 1 min (Figure 9B-II). As aforementioned, an abrupt jump of the reflection wavelength from 560 to 491 nm was found which was caused by the phase transition from BPI to BPII as well (Figure 9B-III).

On the other aspect, a traditional concept indicates that BPLC is alignment-free due to its characteristic of optically isotropy, however the photoresponse of the common BPLC which

is unnecessary for mixing any other functional additives can be attained readily through the photoalignment technique, which can control the orientation direction and surface anchoring through an irradiation, i.e., the lattice orientation of BP at an exposed area shows homogeneity, whereas the common platelet texture, manifesting a random orientation of lattice, is presented at an unexposed area (Figure 9C-I,II).^[63] In virtue of photoalignment, diverse micropatterns with an alternate area of uniform/random orientation of BP lattice, including the straight stripes, squares, fork-like stripes, and even more complicated structures (Figure 9C-III–VI), were formed, and moreover, these patterns were photorewritable due to the feature of photoalignment film. Furthermore, the corresponding diffraction performances of the micropatterns caused by the reflectance contrast between uniform and random-oriented BP zones were detected.

3. Photonic Applications

3.1. Traditional Optics

3.1.1. Microlens Arrays

As sustained efforts have been made to promote the control level of smectic layer curvature, various utilizations based on different types of smectic defects have been developed, including soft-lithographic templates, superhydrophobic surfaces, microlens arrays, and optically selective photomasks.^[6a,10,11] Here, we mainly focus on the applications of self-assembled microlens array based on the smectic FCDs.

Kim et al. presented a microlens array with self-assembled dimple-like TFCDs,^[18] of which the light-focusing ability come from the intrinsic gradient refractive index distribution rather than their geometric shapes. A photolithographically defined Si substrate was prepared with a degenerated planar anchoring condition. Thanks to the rapid responsiveness of the LC molecules, the formation of large-area-ordered TFCDs was simple and fast (a few seconds). The lensing effect of the TFCD array was demonstrated with a microscopic imaging system as shown in **Figure 10A**. Tuning the film thickness of the sample could tailor the domain sizes of TFCDs which consequently determined their focal lengths. Soon after, the same group reported a thermally responsive microlens array within trapezoidal microchannels.^[70] To avoid the sublimation-induced issues of semi-fluorinated SLCs, here a commercial SLC 8CB was used instead to prepare the TFCD array. Because the resultant LC structures in isotropic and nematic phases had no lensing effect, such microlens array could be fast switched between the “on” and “off” states by changing the temperature (Figure 10B), which was very promising in sensors and temperature-dependent optical devices.

By means of the lensing effect of TFCD arrays, optically selective photomasks were proposed.^[71] As shown in Figure 10C-I,II, a typical TFCD structure was composed of a lens region (the central part) and a window region (with flat smectic layers). Generally, the central effective lens region focused light, while the window region of the TFCD was highly transparent. The interesting thing was that when incident light was linearly polarized, due to the specific LC molecular arrangement, the

transmitted light was converged into dumbbell-like spots. This could be verified by the observed pattern on a positive or negative photoresist film. As shown in Figure 10C-IV, the resultant dumbbell-like pattern rather than sharp circular spots was attributed to two facts. One was the anisotropic focusing performance of the TFCD when considering a linearly polarized light, i.e., along the direction of polarization, the gradient refractive index change induced a lens phase profile, while for the direction perpendicular to the polarization, the light perceived similar refractive index and thus the lensing effect was vanished; the other was that the photoresist film was placed away from the focal plane of the microlens array as schematically illustrated in Figure 10C-III. Taking the advantage of this polarization selectivity, one can further infer the incident polarization according to the shapes of the dumbbell-like spots.

On the other hand, Serra and co-workers found the polarization dependence of FCD microlenses with anisotropic geometries.^[72] Such FCDs were produced surrounding cylindrical micropillars with a specific domain size distribution (from the pillar to away from the pillar, the diameters were ranging from a few micrometers up to 30–40 μm). The larger FCDs had high eccentricities compared to the smaller one, and their eccentricity directions (the direction of hyperbola) were radial from the center of the micropillar, which indicated an eccentric refractive index distribution within each FCD. When the polarization was along the hyperbola, light experienced a gradient refractive index, while the refractive index distribution on the perpendicular direction was nearly unchanged. That is the result of the polarization sensitivity. As shown in Figure 10C-V, when the eccentricity directions of FCDs matched the polarization direction, the resultant images were blurred, and the most clear images existed at the direction perpendicular to the polarization. This work provided inspirations for polarization-sensitive microlens design based on the eccentric structures with an anisotropic refractive index distribution.

3.1.2. Beam Steering

Cholesteric helical superstructures with uniform lying helical axes are very suitable to be used as self-assembled phase gratings due to their periodic phase profiles.^[73] Recently, multi-variant controlling methods have been proposed to effectively tune the hierarchical architectures of CLCs.^[39b,74] Accordingly, such CLC gratings are endowed with a wide tunability of grating period and rotation, which is highly promising in beam steering applications.^[75]

Jau and co-authors demonstrated a light-driven CLC grating for beam steering.^[37] The mixture of nematic host E48 and a high HTP azobenzene-based chiral switch was injected into a homogeneous cell. Under the applied voltage of 3.4 V, the CLC grating was formed and its helical pitch could be reversibly tuned in the range of 1.56–2.36 μm during the irradiation of green (532 nm) or violet (405 nm) light (**Figure 11A-I,II**). Correspondingly, its first-order diffraction angle varied from 33° to 54°. In addition, the spectrum scanning function of such photoresponsive CLC grating was also exploited. As schematically illustrated in Figure 11A-III, a white light beam was efficiently dispersed by the CLC sample and selectively detected. A reversible scanning

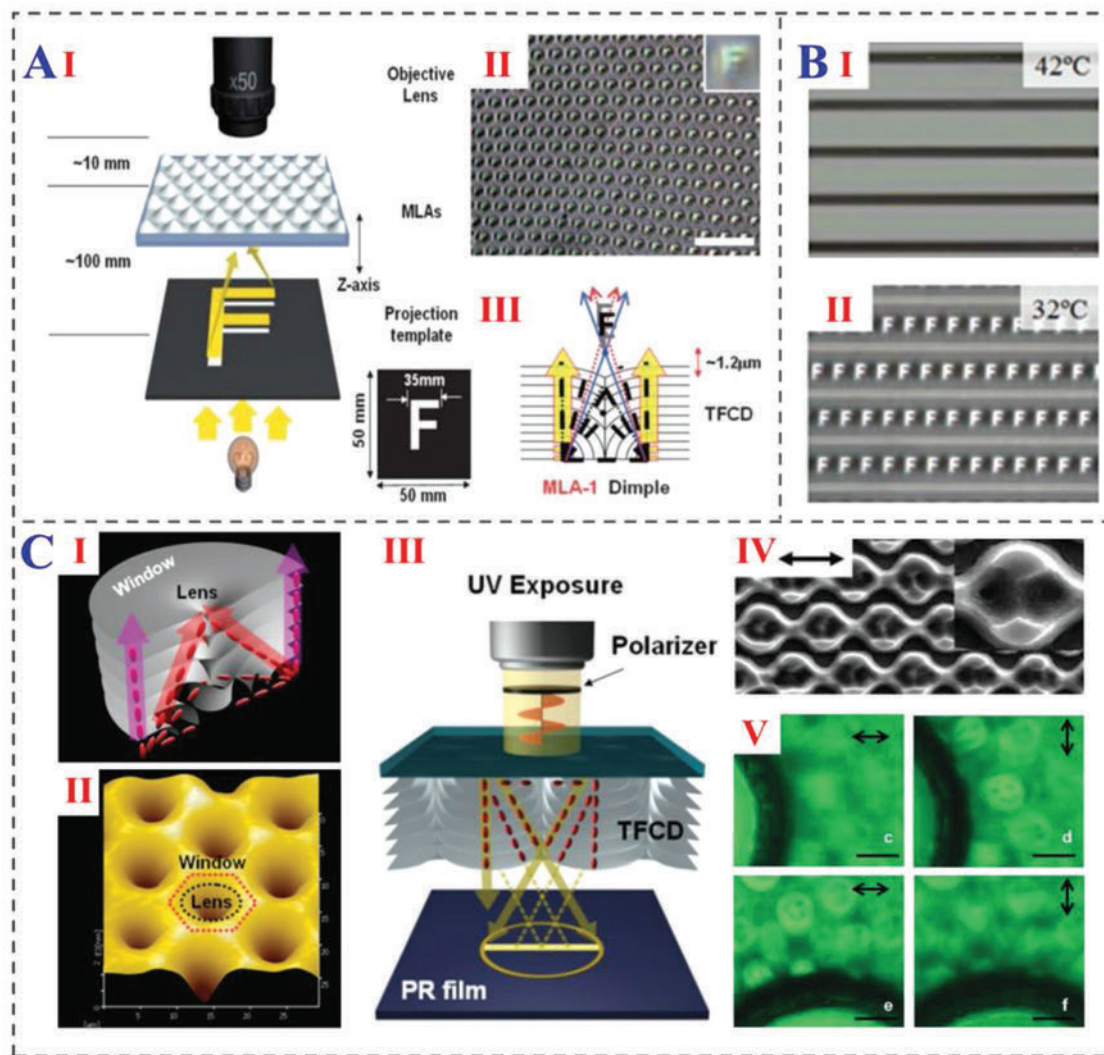


Figure 10. A) Self-assembled TFCD microlens array. I) Experimental setup to demonstrate the lensing effect of TFCDs. II) Imaging pattern of the letter “F” by the TFCD array. III) Schematic illustration of the lensing effect of TFCD. The scale bar indicates 50 mm. B) Thermally responsive TFCD microlens array. I) No lensing effect when the sample was in an isotropic phase (42 °C). II) Imaging pattern of the letter “F” by TFCDs in the smectic phase (32 °C). C) FCD microlens array with a polarization selectivity. I,II) Schematic illustration and AFM image of the TFCD microlens with window and lens regions. III) Schematic illustration of the photolithographic setup with linearly polarized exposure light. IV) Scanning electron microscopy pattern of the positive photoresist generated by the TFCD microlens array. V) Patterns of a smiley face with different polarization states imaged by FCDs at varied positions of the pillar. The scale bars are 30 μm. (A) Reproduced with permission.^[18] Copyright 2010, The Royal Society of Chemistry. (B) Reproduced with permission.^[70] Copyright 2012, The Royal Society of Chemistry. (C-I-IV) Reproduced with permission.^[71] Copyright 2010, Wiley-VCH. (C-V) Reproduced with permission.^[72] Copyright 2015, Wiley-VCH.

wavelength range of 472–713 nm is accomplished via green and violet light stimuli, respectively. This wide-range photo-tunable grating provided new opportunities in light propagation control and spectroscopy applications.^[76]

Ryabchun et al. proposed a rotatable CLC diffraction grating with photoinduced tunable pitch and reversible handedness inversion.^[40b] For this purpose, a photoresponsive CLC was filled into a hybrid cell, resulting in an ordered phase grating. Thanks to the specially designed low-molar-mass CLC mixture, which was composed of a nematic LC ZLI1132 and two dopants MeAzoSorB and LM36 with opposite chirality, photoinvertible handedness inversion of the CLC helical structure could be achieved. Upon the irradiation of UV (365 nm) and visible

(436 nm) lights, clockwise and anticlockwise in-plane rotations of the grating were freely performed (Figure 11B-I). The maximum angle of the continuous rotation has reached about 690° and corresponding diffraction phenomenon was demonstrated (Figure 11B-II).

Similar works on beam steering relying on the handedness inversion of CLC helical superstructure have also been reported. Zheng and co-workers demonstrated a 3D manipulation of the helical axis of a CLC and presented a 2D nonmechanical wide-range beam steering application achieved solely by a light stimulus (Figure 11C-I).^[41b] When the CLC superstructure was at the LH state, the light-activated reversible helical pitch tuning and in-plane rotation of the CLC grating

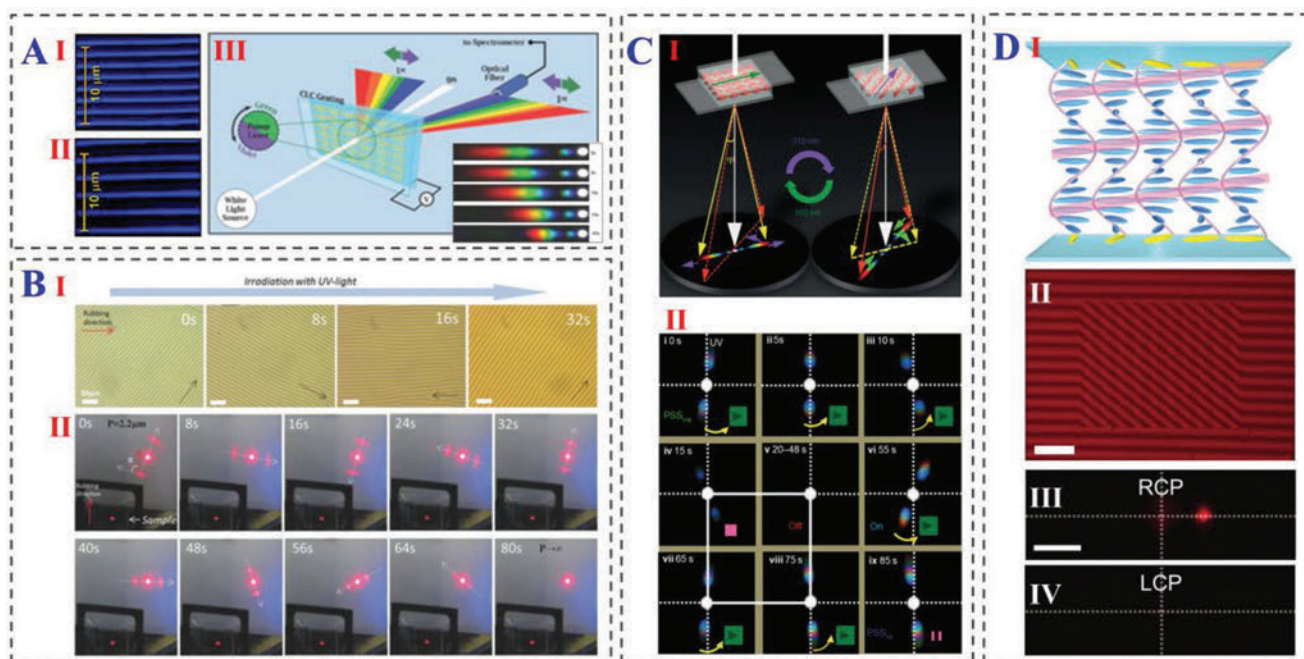


Figure 11. Beam steering via light-activated CLCs. A) Wide-range beam steering and spectrum scanning with a light-activated CLC phase grating. I,II) POM images of the CLC grating tuned by I) green and II) violet light with 3.4 V applied voltage. III) Schematic view of the scanning spectrometer. B) In-plane rotational behaviors of the CLC grating and its corresponding diffraction patterns during the UV light exposure. C) 2D beam steering for spectrum scanning. I) Schematic diagram of the beam steering application. II) 2D beam steering demonstration. D) Reflective deflectors with patterned CLCs. I) Schematic of the LC director distribution. II) Experimental interferograms obtained at ≈ 632 nm. The scale bar is 200 μm . III,IV) Reflected laser spots for opposite circular polarization states of the CLC deflector. The scale bar is 5 mm. (A) Reproduced with permission.^[37] Copyright 2015, Wiley-VCH. (B) Reproduced with permission.^[40b] Copyright 2015, Wiley-VCH. (C) Reproduced with permission.^[41b] Copyright 2017, Nature Publishing Group. (D) Reproduced with permission.^[78] Copyright 2016, Nature Publishing Group.

gave rise to variations of the diffraction angle, thus enabling 2D in-plane beam steering (Figure 11C-II). Moreover, a special bilayer LC cell was also designed and a light-induced diffraction dimensionality transformation was achieved, including 1D and 2D diffraction states and a diffraction off state. The aforementioned photoresponsive materials and controlling methods put forward new strategies for designing controllable diffractive elements as well as their applications.^[77]

The rod-like CLC molecules self-assembling into a periodic helical superstructure contribute to a natural 1D photonic crystal with a helical-variant dielectric tensor.^[7] Thus, for the light propagating along the axis of CLC SH, a broadband Bragg reflection with unique circular-polarization (spin) selectivity occurs over a wavelength range of $n_o p - n_e p$, where n_o and n_e are the ordinary and extraordinary refractive indices, respectively.^[79] The circularly polarized light with the same handedness as the chiral helix of CLCs is reflected, while the other with opposite handedness is transmitted.

In 2016, the spin-orbit geometric phase was discovered from the light reflected off a CLC standing helix.^[78,80] For an inhomogeneously planar aligned CLC, the reflective geometric phase change is twice the orientation angle of local alignment, and possesses a handedness-dependent sign.^[50a,80b] Full phase control of $0-2\pi$ can be expected regardless of any phase retardation condition.^[81] Thanks to the spin-dependent Bragg reflection, such a novel class of optical elements exhibits polarization-determined functionalities and uniform high efficiencies over a broadband ($n_o p - n_e p$).

Via appropriately controlling the spatial distribution of CLC SH, usually through photopatterning technology, a series of planar elements with arbitrary reflected wave-front can be designed. In an initial research work, a periodically rotating CLC helical superstructure (Figure 11D) with a linearly varying phase profile was created using a polarizing projection exposure system.^[78] Such a reflective deflector exhibited nearly 100% diffraction efficiency and large diffraction angle,^[82] showing great potentials in beam steering, optical isolators, 2D/3D wearable displays, and augmented reality displays.^[83]

3.2. Advanced Optics

3.2.1. Specific Optical Field Generation

Besides the light focusing and beam steering applications mentioned above, advanced photonics can be further expected via rationally programming these liquid crystalline hierarchical architectures. Past few years have witnessed a sustained interest and impressive progress in the structured light. Among them, optical vortex (OV) has remained a hot topic of intense scientific curiosity in both classical and quantum optics.^[84] OV possesses a helical phase profile of $e^{im\phi}$ and an orbital angular momentum (OAM) of $m\hbar$ per photon,^[85] where m is the topological charge. As a new degree of freedom to the manipulation of light and thanks to its theoretically infinite eigenstates, OAM has been inspiring fruitful applications such as optical

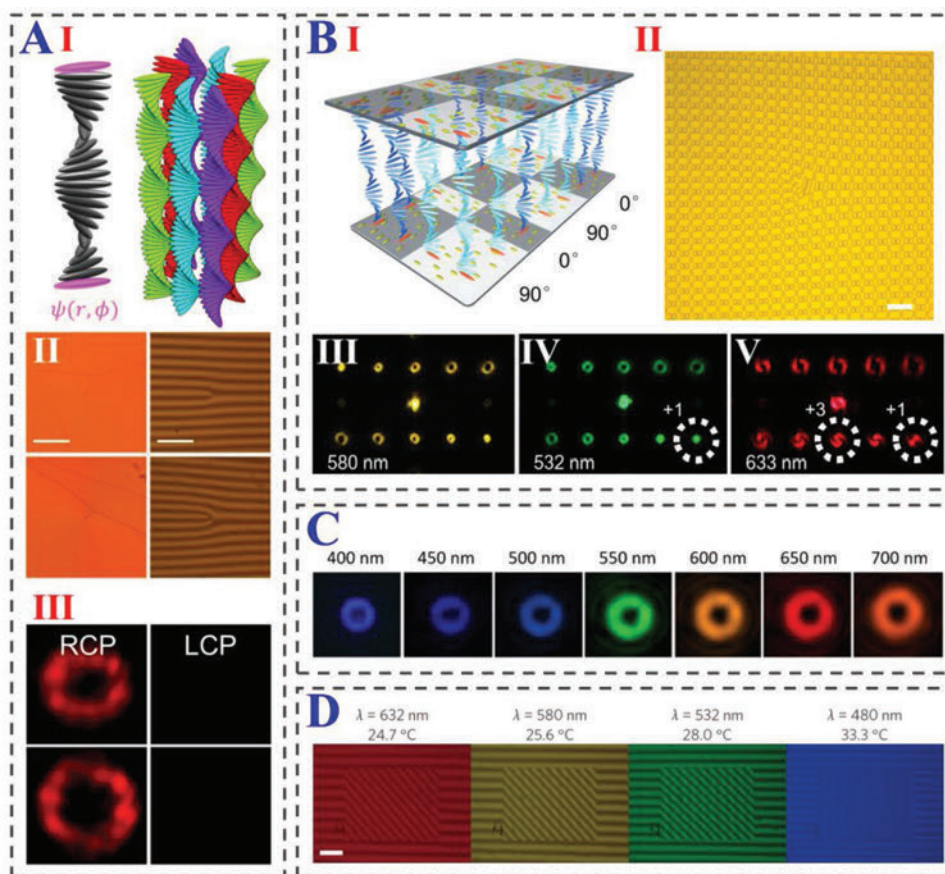


Figure 12. Specific optical field generation via CLC programming. A) CLC q -plates. I) Schematic of the LC director distribution of CLC q -plate. II) Polarized micrographs and measured interferograms. The scale bars are 200 μm . III) Light spot detected by a camera at normal incidence of right/left circular polarization of the CLC q -plates with $q = 0.5$ and $q = 1$. B) A CLC OV processor. I,II) Schematic and micrograph recorded under reflective mode of an optical microscope. The scale bar is 100 μm . III–V) Reflective diffraction patterns for different incident OVs and wavelengths of the CLC Dammann vortex grating. C) Experimental spectral components for far-field intensity profiles of the gradient-pitch CLC q -plate from 400 to 700 nm. D) Temperature-dependent experimental interferograms at different wavelengths of the reflective deflector using temperature-sensitive CLC materials. The scale bar is 200 μm . (A–I) Reproduced with permission.^[96a] Copyright 2017, American Physical Society. (A–II,III) Reproduced with permission.^[90a] Copyright 2016, American Physical Society. (B) Reproduced with permission.^[94] Copyright 2018, Wiley-VCH. (C) Reproduced with permission.^[96a] Copyright 2017, American Physical Society. (D) Reproduced with permission.^[78] Copyright 2016, Nature Publishing Group.

manipulation,^[86] vortex coronagraphy,^[87] optical communications,^[88] and quantum informatics.^[37,89] For all applications above, the OV generation and detection lie at the heart.

Referring to the above principle of CLC reflective geometric phase, a singular point in the spatially patterned helix will bring in high efficiency and polychromatic OV generation (Figure 12A) both at normal and oblique incidences.^[90] The q -plate pattern can be described by $\psi = q\phi$, with a q half-integer and ϕ the azimuthal angle. It has a singular point at the origin and generates an OV with topological charge $m = \pm 2q$.^[91] Broadband reflective OVs have been verified for both diffractive and nondiffractive paraxial light beams,^[90b] either from CLC flat films or droplets.^[80a]

In addition to single OV generation, the concept of digitalized geometric phases^[92] can be introduced for parallel OV manipulation. Through encoding a specific binary pattern,^[93] an innovative CLC OV processor was demonstrated, which was characterized by alternating orthogonal planar alignment (Figure 12B). Up to 25 different OVs were extracted with equal high efficiencies

over a wide wavelength range.^[94] The multiplexed OVs could be distinguished simultaneously without mode crosstalk or distortion, permitting a desirable way for parallel OV processing. To further extend the spectral range, gradient-pitch CLCs were employed, which could be realized by thermal diffusion, slow polymerization, and stacking multiple CLC films with various pitches.^[95] Ultra-broadband OV was obtained in the full visible domain over 400–700 nm range (Figure 12C).^[96] More recently, polychromatic vectorial vortex beams have been presented with the assistant of a rear mirror.^[97] By further combining azimuthal and radial structuring of CLC helix, both scalar and vectorial high-order Laguerre–Gauss beams were generated over a broadband.^[98] These results offer a practical solution to the polychromatic management of the OAM of light.

Thanks to the rapid development of the photopatterning technology,^[81,99] much more complex CLC hierarchical architectures could be flexibly designed and conveniently fabricated. Not only OVs, but also Airy beams,^[100] vortex Airy beams,^[101] and even holograms^[102] could be rationally expected. Especially, different

orientational patterns imprinted on respective substrates would induce the asymmetry depending on the viewing side, resulting in a special semi-transparent and double-sided pseudo-color holograms.^[102] Moreover, such reflective wave-front manipulation can also be achieved in the 3D chiral photonic crystal, BPLC, by controlling the crystal azimuthal orientation.^[50a] The proposed reflective geometric phase modulation is compatible with various CLC functionalization methods. For instance, employing a temperature-sensitive CLC^[103] or a polymer/LC nanocomposite^[104] enables the thermal tunability (Figure 12D) or electric-field switching.^[78] Taking full advantage of the external stimuli response of these soft chiral materials will definitely open a new door toward the active and multifunctional optical devices.

3.2.2. LC Laser Emission

The periodic hierarchical architecture of chiral LCs, whatever the cholesteric phase or the BP, provides a fantastic optical micro-chamber for generating photonic resonance in virtue of its effect of photonic band gap (PBG). As an illuminated dye, having an overlap between its fluorescent spectrum and the PBG, is embedded into such chiral LCs, a laser emission with a narrow bandwidth is generally found under a corresponding light excitation. Tunable performances of a LC laser on both the emission wavelength and the intensity, especially using light as a stimulus, are of prominent significance on the applications of all-optical micro-nano integrated photonics and the development on relevant fields.^[35,105]

Helical pitch can be modulated by light stimulation in a designed photoresponsive chiral LCs system, resulting in the shift of PBG and therefore enabling the tunability of laser emission by light stimulation. Commonly, the photoinsensitive chiral agent, denoted as S811 (left-handedness) or R811 (right-handedness), occurs a reversible photoisomerization by the irradiation of UV light with a shorter wavelength lower than 300 nm, i.e., photo-Fries transformation, which enabled a short-wavelength light-responsive CLC. Herein, a mesogenic rod-like fluorescent dye with its illuminated spectrum covering the near UV to blue-colored visible band was adopted as the gain medium. The PBG shifted about 40 nm under the UV irradiation for 15 min, leading to a modulation of lasing wavelength in a range encompassing more than 30 nm. The recovered process was attained by a stimulation of a visible light with the wavelength of 400–420 nm.^[106] Almost at the same period, another two kinds of phototunable chiral LC systems,^[107] including a photopolymerizable chiral dopant^[107a] and a photolytic cholesteryl iodide, respectively,^[107b] were proposed to implement light tuning of laser emission, which showed a wavelength modulation in the range of 35 nm for the former and 90 nm for the latter. However, the most remarkable problem of such modulations is the irreversible property. Azobenzene-based chiral material thus attracts cumulative attentions due to its reversibility with an alternate irradiation with near UV and green-colored light sources, thereby avoiding the photodegradation of the LCs caused by the deep UV light (i.e., the wavelength lower than 300 nm) and improve the safety of applications.^[108] Results indicated that lasing wavelength was modulated from the initial 667 to 563 nm in less than 20 min by

irradiating with 350 nm UV source, while a complete recovery needed almost 1 day in a dark ambient.

Recently, a unique color cone laser emission was achieved in the case of an oblique incidence of the pumping light with respect to the normal of cell substrates, due to the dependence between the PBG and the impinging direction of pumping light, which displays a symmetric sharp ring pattern and a continuous modulation of the corresponding emission wavelength by varying the incident angle of pumping light.^[109] A phototunable color cone lasing based on CLCs containing photoisomerizable chiral dopant of isosorbide 2,5-bis 4-methoxy-cinnamate exhibited a continuous tuning of emission wavelength covering a spectral range larger than 100 nm, from the original reddish emission to the final green one in 160 s of UV exposure. Such wavelength could be tuned by inclining the cell regarding to the wave vector of pumping light as well.^[110] In addition, a water/oil/water system, containing the aqueous solution of polyvinyl alcohol (PVA) and photoresponsive CLCs, was elaborately prepared, forming a monodispersed CLC micro-shell through the specific designed glass capillary microfluidic device.^[111] Herein, the fluorescent dye was premixed into the CLCs, thereby exhibiting an omnidirectional lasing of such micro photonic shell by suffering a pulsed light stimulation. Such pulsed light acted as not only the laser pumping source, but also the impetus of pitch modulation, thus attaining an interesting dynamic tunable soft core-shell laser emission. To develop an LC film laser, a similar mixture containing aqueous PVA solution and CLCs but with a seriously considered contents, was used to be directly painted on a single substrate and dried as a film at the room temperature in virtue of a deswelling process of the mixture. As aforementioned, the similar gain medium and azobenzene-based chiral molecular switch were homogeneously mixed into the system, thus realizing a light reversible tunable laser film displaying a wide tuning spectral range from 566 to 678 nm.^[112]

4. Summary and Perspective

Since the advent of LC displays in 1970s and the subsequent large-scale production 20 years ago, nematic LC attracts accumulative attentions and is recognized as a promising optical functional material. Hierarchical architecture is very ubiquitous in LC relevant soft materials which are mainly formed through molecular self-organization, such as the cholesteric phase which is actually the first LC phase found in 150 years ago, the smectic phase featuring a 2D ordered layer close to the arrangement of a crystal, and the BP manifesting 3D cubic structure stacked by double twisted arranged hierarchical LCs. However, substantial progresses on photoactivity of such LC superstructures, whatever its fundamental mechanisms and potential applications, are not extensively exploited until the recent decade thanks to the remarkable developments on the progresses of materials and techniques. The flexible smectic layer curvature control is accomplished via 2D anchoring and 3D topographic confinement, and can be further tuned by external fields. The generation of periodic FCD arrays with controllable domain size, shape, orientation, and lattice symmetry can be achieved conveniently. Regarding to the helical axis manipulation of CLCs and the hierarchical architecture of BPLCs, approaches based

on the photoalignment technique as well as various light-driven azobenzene molecular motors are exploited. Impressively, the 3D manipulation and handedness inversion of CLC of the helical axis are realized with a facile light stimulus. Such new concept insights become a strong impetus that promotes scientists to re-examine and reconsider some profound issues in science and engineering, which is our motivation to write this review. In addition, diverse advanced photonic applications, including microlens arrays, beam steering, special optical field generation, and LC lasers, are presented briefly and systematically.

Photoactivated hierarchical architecture of LC has inevitably been a thriving topic of LC relevant researches and is experiencing a development by leaps and bounds. However, it is noteworthy that plentiful of problematic and intractable fundamental difficulties, such as the kinetics in the process of light stimulations, the self-organization behaviors, and the photon transferring and interaction in such an elegant and fantastic soft architecture and the modulation of the hierarchical structure to photons, still deserve an urgent further study. Furthermore, developing new photoactivated superstructures which have strong fatigue resistance and weak thermal relaxation, is the only road leads to Rome, i.e., the applications with excellent photoreponsive performance. Photonic application of photoactivated hierarchical LC architecture is definitely not the only application, the characteristics of soft, photoresponsive, and self-organized periodic microstructures will indeed set off an application storm toward a broader field beyond photonics, such as soft materials, green energetics, biology, and even fluid mechanics.

Acknowledgements

L.L.M., W.H., Z.G.Z. contributed equally to this work. This work was supported by the National Natural Science Foundation of China (NSFC) (nos. 61435008 and 61490714), the Distinguished Young Scholars Fund of Jiangsu Province (BK20180004), and the Scientific Research Foundation of Graduate School of Nanjing University (2017ZDL06). W.H. gratefully acknowledges the support of the Tang Scholar program.

Conflict of Interest

The authors declare no conflict of interest.

Keywords

hierarchical superstructures, light-activated phenomena, liquid crystals, photonics

Received: March 4, 2019

Revised: April 11, 2019

Published online:

- [1] a) M. Thomé, L. Nicole, S. Berthier, *Mater. Today* **2014**, *1*, 221; b) S. Yoshioka, S. Kinoshita, *Forma* **2002**, *17*, 169.
[2] Y. T. Cheng, D. E. Rodak, C. A. Wong, C. A. Hayden, *Nanotechnology* **2006**, *17*, 1359.
[3] X. Gao, L. Jiang, *Nature* **2004**, *432*, 36.

- [4] C. Zhang, D. A. McAdams li, J. C. Grunlan, *Adv. Mater.* **2016**, *28*, 6292.
[5] a) D. B. Liarte, M. Bierbaum, R. A. Mosna, R. D. Kamien, J. P. Sethna, *Phys. Rev. Lett.* **2016**, *116*, 147802; b) D. K. Yoon, Y. H. Kim, D. S. Kim, S. D. Oh, I. I. Smalyukh, N. A. Clark, H. T. Jung, *Proc. Natl. Acad. Sci. U. S. A.* **2013**, *110*, 19263; c) O. D. Lavrentovich, *Proc. Natl. Acad. Sci. U. S. A.* **2013**, *110*, 5.
[6] a) Y. H. Kim, D. K. Yoon, H. S. Jeong, O. D. Lavrentovich, H.-T. Jung, *Adv. Funct. Mater.* **2011**, *21*, 610; b) D. S. Kim, Y. J. Cha, M. H. Kim, O. D. Lavrentovich, D. K. Yoon, *Nat. Commun.* **2016**, *7*, 10236; c) A. Honglawan, D. A. Beller, M. Cavallaro, R. D. Kamien, K. J. Stebe, S. Yang, *Proc. Natl. Acad. Sci. U. S. A.* **2013**, *110*, 34; d) M. C. Choi, T. Pfohl, Z. Wen, Y. Li, M. W. Kim, J. N. Israelachvili, C. R. Safinya, *Proc. Natl. Acad. Sci. U. S. A.* **2004**, *101*, 17340.
[7] I.-C. Khoo, S.-T. Wu, *Optics and Nonlinear Optics of Liquid Crystals*, World Scientific, Singapore **1993**.
[8] a) D. C. Wright, N. D. Mermin, *Rev. Mod. Phys.* **1989**, *61*, 385; b) H. Kikuchi, in *Liquid Crystalline Functional Assemblies and Their Supramolecular Structures* (Ed: T. Kato), Structure and Bonding, Vol. 128, Springer, Berlin, Heidelberg **2007**, p. 99.
[9] L. Wang, K. G. Gutierrez-Cuevas, H. K. Bisoyi, J. Xiang, G. Singh, R. S. Zola, S. Kumar, O. D. Lavrentovich, A. Urbas, Q. Li, *Chem. Commun.* **2015**, *51*, 15039.
[10] L. Wang, Q. Li, *Adv. Funct. Mater.* **2016**, *26*, 10.
[11] A. Honglawan, S. Yang, in *Nanoscience with Liquid Crystals: From Self-Organized Nanostructures to Applications* (Ed: Q. Li), NanoScience and Technology, Vol. 26, Springer International Publishing, Switzerland **2014**, p. 35.
[12] G. Darboux, *Principes de Géométrie Analytique*, Gauthier-Villars, Paris **1917**.
[13] J. M. Ok, Y. H. Kim, H. S. Jeong, H. W. Yoo, J. H. Kim, M. Srinivasarao, H. T. Jung, *Soft Matter* **2013**, *9*, 10135.
[14] M. Kleman, O. D. Lavrentovich, *Soft Matter Physics: An Introduction*, Springer-Verlag, New York **2003**.
[15] M. Kleman, O. D. Lavrentovich, *Liq. Cryst.* **2009**, *36*, 1085.
[16] Y. H. Kim, D. K. Yoon, H. S. Jeong, H. T. Jung, *Soft Matter* **2010**, *6*, 1426.
[17] Y. H. Kim, D. K. Yoon, H. S. Jeong, J. H. Kim, E. K. Yoon, H. T. Jung, *Adv. Funct. Mater.* **2009**, *19*, 3008.
[18] Y. H. Kim, H. S. Jeong, J. H. Kim, E. K. Yoon, D. K. Yoon, H. T. Jung, *J. Mater. Chem.* **2010**, *20*, 6557.
[19] D. K. Yoon, M. Choi, Y. H. Kim, M. W. Kim, O. D. Lavrentovich, H.-T. Jung, *Nat. Mater.* **2007**, *6*, 866.
[20] J. M. Ok, Y. H. Kim, T. Y. Lee, H. W. Yoo, K. Kwon, W. B. Jung, S. H. Kim, H. T. Jung, *Langmuir* **2016**, *32*, 13418.
[21] L. L. Ma, M. J. Tang, W. Hu, Z. Q. Cui, S. J. Ge, P. Chen, L. J. Chen, H. Qian, L. F. Chi, Y. Q. Lu, *Adv. Mater.* **2017**, *29*, 1606671.
[22] a) B. Y. Wei, W. Hu, Y. Ming, F. Xu, S. Rubin, J. G. Wang, V. G. Chigrinov, Y. Q. Lu, *Adv. Mater.* **2014**, *26*, 1590; b) H. Wu, W. Hu, H. C. Hu, X. W. Lin, G. Zhu, J. W. Choi, V. G. Chigrinov, Y. Q. Lu, *Opt. Express* **2012**, *20*, 16684.
[23] M. J. Shin, M. J. Gim, D. K. Yoon, *Langmuir* **2018**, *34*, 2551.
[24] N. Pivovarova, I. Boldescul, O. Lavrentovich, S. Shelyazhenko, Y. Fialkov, *Kristallografiya* **1988**, *33*, 1460.
[25] J. H. Kim, Y. H. Kim, H. S. Jeong, E. K. Yoon, H. T. Jung, *J. Mater. Chem.* **2011**, *21*, 18381.
[26] A. Honglawan, D. A. Beller, M. Cavallaro, R. D. Kamien, K. J. Stebe, S. Yang, *Adv. Mater.* **2011**, *23*, 5519.
[27] Y. H. Kim, D. K. Yoon, M. C. Choi, H. S. Jeong, M. W. Kim, O. D. Lavrentovich, H. T. Jung, *Langmuir* **2009**, *25*, 1685.
[28] a) M. J. Gim, D. K. Yoon, *ACS Appl. Mater. Interfaces* **2016**, *8*, 27942; b) A. Suh, H. Ahn, T. J. Shin, D. K. Yoon, *J. Mater. Chem. C* **2019**, *7*, 1713; c) I. Gryn, E. Lacaze, R. Bartolino, B. Zappone, *Adv. Funct. Mater.* **2015**, *25*, 142; d) I. Gryn, E. Lacaze, L. Carbone, M. Giocondo, B. Zappone, *Adv. Funct. Mater.* **2016**, *26*, 7122.

- [29] D. S. Kim, D. K. Yoon, *J. Inf. Disp.* **2018**, *19*, 7.
- [30] a) S. W. Kang, S. Sprunt, L. C. Chien, *Appl. Phys. Lett.* **2000**, *76*, 3516; b) S.-W. Kang, S. Sprunt, L.-C. Chien, *Chem. Mater.* **2006**, *18*, 4436; c) W.-S. Li, L.-L. Ma, L.-L. Gong, S.-S. Li, C. Yang, B. Luo, W. Hu, L.-J. Chen, *Opt. Mater. Express* **2016**, *6*, 19.
- [31] a) J. Xiang, S. V. Shiyankovskii, Y. Li, C. T. Imrie, Q. Li, O. D. Lavrentovich, presented at *Proc. SPIE Organic Photonics and Electronics: Liquid Crystals XVIII*, San Diego, CA, United States, October **2014**; b) I. Gvozdevskyy, O. Yaroshchuk, M. Serbina, R. Yamaguchi, *Opt. Express* **2012**, *20*, 3499.
- [32] a) T. Nose, T. Miyashishi, Y. Aizawa, R. Ito, M. Honma, *Jpn. J. Appl. Phys.* **2010**, *49*, 051701; b) J. Baudry, M. Brazovskaia, L. Lejcek, P. Oswald, S. Pirkel, *Liq. Cryst.* **1996**, *21*, 893.
- [33] a) M. Moirangthem, R. Arts, M. Merckx, A. P. Schenning, *Adv. Funct. Mater.* **2016**, *26*, 1154; b) J. Tian, Y. He, J. Li, J. Wei, G. Li, J. Guo, *Adv. Opt. Mater.* **2018**, *6*, 1701337.
- [34] J. Li, H. K. Bisoyi, J. Tian, J. Guo, Q. Li, *Adv. Mater.* **2019**, *31*, 1807751.
- [35] H. Coles, S. Morris, *Nat. Photonics* **2010**, *4*, 676.
- [36] H. Khandelwal, A. P. Schenning, M. G. Debije, *Adv. Energy Mater.* **2017**, *7*, 1602209.
- [37] H. C. Jau, Y. Li, C. C. Li, C. W. Chen, C. T. Wang, H. K. Bisoyi, T. H. Lin, T. J. Bunning, Q. Li, *Adv. Opt. Mater.* **2015**, *3*, 166.
- [38] a) J. Lub, P. Van De Witte, C. Doornkamp, J. P. Vogels, R. T. Wegh, *Adv. Mater.* **2003**, *15*, 1420; b) N. Y. Ha, Y. Ohtsuka, S. M. Jeong, S. Nishimura, G. Suzuki, Y. Takahashi, K. Ishikawa, H. Takezoe, *Nat. Mater.* **2008**, *7*, 43.
- [39] a) L.-L. Ma, S.-S. Li, W.-S. Li, W. Ji, B. Luo, Z.-G. Zheng, Z.-P. Cai, V. Chigrinov, Y.-Q. Lu, W. Hu, L.-J. Chen, *Adv. Opt. Mater.* **2015**, *3*, 1691; b) A. Ryabchun, A. Bobrovsky, J. Stumpe, V. Shibaev, *Adv. Opt. Mater.* **2015**, *3*, 1462.
- [40] a) S.-S. Li, Y. Shen, Z.-N. Chang, W.-S. Li, Y.-C. Xu, X.-Y. Fan, L.-J. Chen, *Appl. Phys. Lett.* **2017**, *111*, 231109; b) A. Ryabchun, A. Bobrovsky, J. Stumpe, V. Shibaev, *Adv. Opt. Mater.* **2015**, *3*, 1273.
- [41] a) R. Eelkema, M. M. Pollard, J. Vicario, N. Katsonis, B. S. Ramon, C. W. Bastiaansen, D. J. Broer, B. L. Feringa, *Nature* **2006**, *440*, 163; b) Z.-G. Zheng, Y. Li, H. K. Bisoyi, L. Wang, T. J. Bunning, Q. Li, *Nature* **2016**, *531*, 352.
- [42] O. Yaroshchuk, Y. Reznikov, *J. Mater. Chem.* **2012**, *22*, 286.
- [43] H.-C. Yeh, G.-H. Chen, C.-R. Lee, T.-S. Mo, *Appl. Phys. Lett.* **2007**, *90*, 261103.
- [44] a) Y. Wang, Q. Li, *Adv. Mater.* **2012**, *24*, 1926; b) Y. Kim, N. Tamaoki, *J. Mater. Chem. C* **2014**, *2*, 9258; c) J. Li, Z. Zhang, J. Tian, G. Li, J. Wei, J. Guo, *Adv. Opt. Mater.* **2017**, *5*, 1700014.
- [45] F. Kimura, T. Kimura, M. Tamura, A. Hirai, M. Ikuno, F. Horii, *Langmuir* **2005**, *21*, 2034.
- [46] a) R. Eelkema, M. M. Pollard, N. Katsonis, J. Vicario, D. J. Broer, B. L. Feringa, *J. Am. Chem. Soc.* **2006**, *128*, 14397; b) A. Bosco, M. G. Jongejan, R. Eelkema, N. Katsonis, E. Lacaze, A. Ferrarini, B. L. Feringa, *J. Am. Chem. Soc.* **2008**, *130*, 14615; c) H. Ayeb, J. Grand, H. Sellame, S. Truong, J. Aubard, N. Felidj, A. Mlayah, E. Lacaze, *J. Mater. Chem.* **2012**, *22*, 7856.
- [47] L.-L. Ma, W. Duan, M.-J. Tang, L.-J. Chen, X. Liang, Y.-Q. Lu, W. Hu, *Polymers* **2017**, *9*, 295.
- [48] J. Yan, L. Rao, M. Jiao, Y. Li, H.-C. Cheng, S.-T. Wu, *J. Mater. Chem.* **2011**, *21*, 7870.
- [49] a) S. Yokoyama, S. Mashiko, H. Kikuchi, K. Uchida, T. Nagamura, *Adv. Mater.* **2006**, *18*, 48; b) W. Cao, A. Muñoz, P. Palffy-Muhoray, B. Taheri, *Nat. Mater.* **2002**, *1*, 111.
- [50] a) H. Yoshida, J. Kobashi, *Liq. Cryst.* **2016**, *43*, 1909; b) J. Guo, J. Wang, J. Zhang, Y. Shi, X. Wang, J. Wei, *J. Mater. Chem. C* **2014**, *2*, 9159.
- [51] a) J. Yan, S.-T. Wu, *Opt. Mater. Express* **2011**, *1*, 1527; b) H. J. Coles, M. N. Pivnenko, *Nature* **2005**, *436*, 997.
- [52] a) J. Sun, S.-T. Wu, *J. Polym. Sci., Part B: Polym. Phys.* **2014**, *52*, 183; b) Y. Li, S. Huang, P. Zhou, S. Liu, J. Lu, X. Li, Y. Su, *Adv. Mater. Technol.* **2016**, *1*, 1600102.
- [53] a) H. K. Bisoyi, Q. Li, *Acc. Chem. Res.* **2014**, *47*, 3184; b) H. K. Bisoyi, Q. Li, *Angew. Chem., Int. Ed.* **2016**, *55*, 2994; c) H. K. Bisoyi, Q. Li, *Chem. Rev.* **2016**, *116*, 15089.
- [54] A. Chanishvili, G. Chilaya, G. Petriashvili, P. J. Collings, *Phys. Rev. E* **2005**, *71*, 051705.
- [55] H.-Y. Liu, C.-T. Wang, C.-Y. Hsu, T.-H. Lin, J.-H. Liu, *Appl. Phys. Lett.* **2010**, *96*, 121103.
- [56] R. J. Miller, H. F. Gleeson, *J. Phys. II* **1996**, *6*, 909.
- [57] R. K. Vijayaraghavan, S. Abraham, D. S. Rao, S. K. Prasad, S. Das, *Chem. Commun.* **2010**, *46*, 2796.
- [58] K. Zhou, H. K. Bisoyi, J. Q. Jin, C. L. Yuan, Z. Liu, D. Shen, Y. Q. Lu, Z. G. Zheng, W. Zhang, Q. Li, *Adv. Mater.* **2018**, *30*, 1800237.
- [59] T. H. Lin, Y. Li, C. T. Wang, H. C. Jau, C. W. Chen, C. C. Li, H. K. Bisoyi, T. J. Bunning, Q. Li, *Adv. Mater.* **2013**, *25*, 5050.
- [60] O. Jin, D. Fu, J. Wei, H. Yang, J. Guo, *RSC Adv.* **2014**, *4*, 28597.
- [61] W.-L. He, M. Li, S.-Q. Liu, M.-J. Wei, C. Liu, L.-L. Li, Z. Yang, D. Wang, H. Cao, *Liq. Cryst.* **2018**, *45*, 370.
- [62] M. J. Gim, S. T. Hur, K. W. Park, M. Lee, S. W. Choi, H. Takezoe, *Chem. Commun.* **2012**, *48*, 9968.
- [63] Z. G. Zheng, C. L. Yuan, W. Hu, H. K. Bisoyi, M. J. Tang, Z. Liu, P. Z. Sun, W. Q. Yang, X. Q. Wang, D. Shen, *Adv. Mater.* **2017**, *29*, 1703165.
- [64] a) L. Wang, W. He, X. Xiao, F. Meng, Y. Zhang, P. Yang, L. Wang, J. Xiao, H. Yang, Y. Lu, *Small* **2012**, *8*, 2189; b) F. Castles, S. M. Morris, J. M. Hung, M. M. Qasim, A. D. Wright, S. Nosheen, S. S. Choi, B. I. Outram, S. J. Elston, C. Burgess, L. Hill, T. D. Wilkinson, H. J. Coles, *Nat. Mater.* **2014**, *13*, 817; c) J. Wang, C.-G. Lin, J. Zhang, J. Wei, Y.-F. Song, J. Guo, *J. Mater. Chem. C* **2015**, *3*, 4179.
- [65] a) M. Nakata, Y. Takahashi, J. Watanabe, H. Takezoe, *Phys. Rev. E* **2003**, *68*, 041710; b) Z. Zheng, D. Shen, P. Huang, *New J. Phys.* **2010**, *12*, 113018; c) H. Wang, Z. Zheng, D. Shen, *Liq. Cryst.* **2012**, *39*, 99; d) L. Wang, W. He, X. Xiao, M. Wang, M. Wang, P. Yang, Z. Zhou, H. Yang, H. Yu, Y. Lu, *J. Mater. Chem.* **2012**, *22*, 19629; e) W.-Q. Yang, G.-Q. Cai, Z. Liu, X.-Q. Wang, W. Feng, Y. Feng, D. Shen, Z.-G. Zheng, *J. Mater. Chem. C* **2017**, *5*, 690.
- [66] a) Y. Wu, Y. Zhou, L. Yin, G. Zou, Q. Zhang, *Liq. Cryst.* **2013**, *40*, 726; b) Y. Wen, Z. Zheng, H. Wang, D. Shen, *Liq. Cryst.* **2012**, *39*, 509.
- [67] M. Wang, W. Hu, L. Wang, D.-Y. Guo, T.-H. Lin, L. Zhang, H. Yang, *J. Mater. Chem. C* **2018**, *6*, 7740.
- [68] L. Wang, H. Dong, Y. Li, C. Xue, L.-D. Sun, C.-H. Yan, Q. Li, *J. Am. Chem. Soc.* **2014**, *136*, 4480.
- [69] a) K. G. Gutierrez-Cuevas, L. Wang, C. Xue, G. Singh, S. Kumar, A. Urbas, Q. Li, *Chem. Commun.* **2015**, *51*, 9845; b) L. Wang, H. K. Bisoyi, Z. Zheng, K. G. Gutierrez-Cuevas, G. Singh, S. Kumar, T. J. Bunning, Q. Li, *Mater. Today* **2017**, *20*, 230.
- [70] J. H. Kim, Y. H. Kim, H. S. Jeong, M. Srinivasarao, S. D. Hudson, H.-T. Jung, *RSC Adv.* **2012**, *2*, 6729.
- [71] Y. H. Kim, J. O. Lee, H. S. Jeong, J. H. Kim, E. K. Yoon, D. K. Yoon, J. B. Yoon, H. T. Jung, *Adv. Mater.* **2010**, *22*, 2416.
- [72] F. Serra, M. A. Gharbi, Y. Luo, I. B. Liu, N. D. Bade, R. D. Kamien, S. Yang, K. J. Stebe, *Adv. Opt. Mater.* **2015**, *3*, 1287.
- [73] a) I. A. Yao, C.-H. Liaw, S.-H. Chen, J.-J. Wu, *J. Appl. Phys.* **2004**, *96*, 1760; b) W.-C. Hung, W.-H. Cheng, M.-S. Tsai, Y.-C. Juan, I. M. Jiang, P. Yeh, *Appl. Phys. Lett.* **2007**, *90*, 183115; c) H.-C. Jau, T.-H. Lin, Y.-Y. Chen, C.-W. Chen, J.-H. Liu, A. Y. G. Fuh, *Appl. Phys. Lett.* **2012**, *100*, 131909.
- [74] C.-H. Lin, R.-H. Chiang, S.-H. Liu, C.-T. Kuo, C.-Y. Huang, *Opt. Express* **2012**, *20*, 26837.
- [75] L. Zhang, L. Wang, U. S. Hiremath, H. K. Bisoyi, G. G. Nair, C. V. Yelamagad, A. M. Urbas, T. J. Bunning, Q. Li, *Adv. Mater.* **2017**, *29*, 1700676.

- [76] D. Subacius, S. V. Shiyankovskii, P. Bos, O. D. Lavrentovich, *Appl. Phys. Lett.* **1997**, *71*, 3323.
- [77] C.-C. Li, C.-W. Chen, C.-K. Yu, H.-C. Jau, J.-A. Lv, X. Qing, C.-F. Lin, C.-Y. Cheng, C.-Y. Wang, J. Wei, Y. Yu, T.-H. Lin, *Adv. Opt. Mater.* **2017**, *5*, 1600824.
- [78] J. Kobashi, H. Yoshida, M. Ozaki, *Nat. Photonics* **2016**, *10*, 389.
- [79] P. Yeh, C. Gu, *Optics of Liquid Crystal Displays*, John Wiley & Sons, New York **1999**.
- [80] a) M. Rafayelyan, G. Tkachenko, E. Brasselet, *Phys. Rev. Lett.* **2016**, *116*, 253902; b) R. Barboza, U. Bortolozzo, M. G. Clerc, S. Residori, *Phys. Rev. Lett.* **2016**, *117*, 053903.
- [81] J. Kim, Y. Li, M. N. Miskiewicz, C. Oh, M. W. Kudenov, M. J. Escuti, *Optica* **2015**, *2*, 958.
- [82] a) Y. Weng, D. Xu, Y. Zhang, X. Li, S. T. Wu, *Opt. Express* **2016**, *24*, 17746; b) J. Kobashi, Y. Mohri, H. Yoshida, M. Ozaki, *Opt. Data Process. Storage* **2017**, *3*, 61.
- [83] Y.-H. Lee, K. Yin, S.-T. Wu, *Opt. Express* **2017**, *25*, 27008.
- [84] a) S. Franke-Arnold, L. Allen, M. Padgett, *Laser Photonics Rev.* **2008**, *2*, 299; b) A. M. Yao, M. J. Padgett, *Adv. Opt. Photonics* **2011**, *3*, 161; c) R. Barboza, U. Bortolozzo, M. G. Clerc, S. Residori, E. Vidal-Henriquez, *Adv. Opt. Photonics* **2015**, *7*, 635.
- [85] L. Allen, M. W. Beijersbergen, R. Spreeuw, J. Woerdman, *Phys. Rev. A* **1992**, *45*, 8185.
- [86] M. Padgett, R. Bowman, *Nat. Photonics* **2011**, *5*, 343.
- [87] A. Aleksanyan, N. Kravets, E. Brasselet, *Phys. Rev. Lett.* **2017**, *118*, 203902.
- [88] a) J. Wang, J.-Y. Yang, I. M. Fazal, N. Ahmed, Y. Yan, H. Huang, Y. Ren, Y. Yue, S. Dolinar, M. Tur, *Nat. Photonics* **2012**, *6*, 488; b) A. E. Willner, H. Huang, Y. Yan, Y. Ren, N. Ahmed, G. Xie, C. Bao, L. Li, Y. Cao, Z. Zhao, *Adv. Opt. Photonics* **2015**, *7*, 66.
- [89] F. Cardano, A. D'Errico, A. Dauphin, M. Maffei, B. Piccirillo, C. de Lisio, G. De Filippis, V. Cataudella, E. Santamato, L. Marrucci, *Nat. Commun.* **2017**, *8*, 15516.
- [90] a) J. Kobashi, H. Yoshida, M. Ozaki, *Phys. Rev. Lett.* **2016**, *116*, 253903; b) M. Rafayelyan, E. Brasselet, *Opt. Lett.* **2016**, *41*, 3972; c) T. Lin, Y. Zhou, Y. Yuan, W. Fu, L. Yao, H. Huang, F. Fan, S. Wen, *Opt. Express* **2018**, *26*, 29244.
- [91] a) L. Marrucci, C. Manzo, D. Paparo, *Phys. Rev. Lett.* **2006**, *96*, 163905; b) P. Chen, W. Ji, B.-Y. Wei, W. Hu, V. Chigrinov, Y.-Q. Lu, *Appl. Phys. Lett.* **2015**, *107*, 241102.
- [92] a) P. Chen, S.-J. Ge, W. Duan, B.-Y. Wei, G.-X. Cui, W. Hu, Y.-Q. Lu, *ACS Photonics* **2017**, *4*, 1333; b) R. Xu, P. Chen, J. Tang, W. Duan, S.-J. Ge, L.-L. Ma, R.-X. Wu, W. Hu, Y.-Q. Lu, *Phys. Rev. Appl.* **2018**, *10*, 034061.
- [93] a) S.-J. Ge, P. Chen, L.-L. Ma, Z. Liu, Z.-G. Zheng, D. Shen, W. Hu, Y.-Q. Lu, *Opt. Mater. Express* **2016**, *6*, 1087; b) P. Chen, S.-J. Ge, L.-L. Ma, W. Hu, V. Chigrinov, Y.-Q. Lu, *Phys. Rev. Appl.* **2016**, *5*, 044009.
- [94] P. Chen, L. L. Ma, W. Duan, J. Chen, S. J. Ge, Z. H. Zhu, M. J. Tang, R. Xu, W. Gao, T. Li, *Adv. Mater.* **2018**, *30*, 1705865.
- [95] M. Mitov, *Adv. Mater.* **2012**, *24*, 6260.
- [96] a) M. Rafayelyan, G. Agez, E. Brasselet, *Phys. Rev. A* **2017**, *96*, 043862; b) J. Kobashi, H. Yoshida, M. Ozaki, *Mol. Cryst. Liq. Cryst.* **2017**, *646*, 116.
- [97] M. Rafayelyan, E. Brasselet, *Phys. Rev. Lett.* **2018**, *120*, 213903.
- [98] M. G. Nassiri, S. Y. Cho, H. Yoshida, M. Ozaki, E. Brasselet, *Phys. Rev. A* **2018**, *98*, 063834.
- [99] a) P. Chen, B. Y. Wei, W. Ji, S. J. Ge, W. Hu, F. Xu, V. G. Chigrinov, Y. Q. Lu, *Photonics Res.* **2015**, *3*, 133; b) Y. Guo, M. Jiang, C. Peng, K. Sun, O. Yaroshchuk, O. Lavrentovich, Q. H. Wei, *Adv. Mater.* **2016**, *28*, 2353.
- [100] a) G. Siviloglou, J. Broky, A. Dogariu, D. Christodoulides, *Phys. Rev. Lett.* **2007**, *99*, 213901; b) B.-Y. Wei, P. Chen, W. Hu, W. Ji, L.-Y. Zheng, S.-J. Ge, Y. Ming, V. Chigrinov, Y.-Q. Lu, *Sci. Rep.* **2015**, *5*, 17484.
- [101] a) B.-Y. Wei, P. Chen, S.-J. Ge, W. Duan, W. Hu, Y.-Q. Lu, *Appl. Phys. Lett.* **2016**, *109*, 121105; b) B.-Y. Wei, S. Liu, P. Chen, S.-X. Qi, Y. Zhang, W. Hu, Y.-Q. Lu, J.-L. Zhao, *Appl. Phys. Lett.* **2018**, *112*, 121101.
- [102] J. Kobashi, H. Yoshida, M. Ozaki, *Sci. Rep.* **2017**, *7*, 16470.
- [103] Y. Huang, Y. Zhou, C. Doyle, S.-T. Wu, *Opt. Express* **2006**, *14*, 1236.
- [104] Y. Inoue, H. Yoshida, H. Kubo, M. Ozaki, *Adv. Opt. Mater.* **2013**, *1*, 256.
- [105] a) J. Hwang, M. H. Song, B. Park, S. Nishimura, T. Toyooka, J. W. Wu, Y. Takanishi, K. Ishikawa, H. Takezoe, *Nat. Mater.* **2005**, *4*, 383; b) A. D. Ford, S. M. Morris, H. J. Coles, *Mater. Today* **2006**, *9*, 36.
- [106] A. Chanishvili, G. Chilaya, G. Petriashvili, R. Barberi, R. Bartolino, G. Cipparrone, A. Mazzulla, L. Oriol, *Appl. Phys. Lett.* **2003**, *83*, 5353.
- [107] a) A. Y.-G. Fuh, T.-H. Lin, J.-H. Liu, F.-C. Wu, *Opt. Express* **2004**, *12*, 1857; b) S. Furumi, S. Yokoyama, A. Otomo, S. Mashiko, *Appl. Phys. Lett.* **2004**, *84*, 2491.
- [108] a) G. Chilaya, A. Chanishvili, G. Petriashvili, R. Barberi, R. Bartolino, G. Cipparrone, A. Mazzulla, P. V. Shibaev, *Adv. Mater.* **2007**, *19*, 565; b) P. V. Shibaev, R. L. Sanford, D. Chiappetta, V. Milner, A. Genack, A. Bobrovsky, *Opt. Express* **2005**, *13*, 2358.
- [109] a) C.-R. Lee, S.-H. Lin, H.-C. Yeh, T.-D. Ji, K.-L. Lin, T.-S. Mo, C.-T. Kuo, K.-Y. Lo, S.-H. Chang, A. Y.-G. Fuh, *Opt. Express* **2009**, *17*, 12910; b) C.-R. Lee, S.-H. Lin, H.-C. Yeh, T.-D. Ji, *Opt. Express* **2009**, *17*, 22616.
- [110] J. D. Lin, M. H. Hsieh, G. J. Wei, T. S. Mo, S. Y. Huang, C. R. Lee, *Opt. Express* **2013**, *21*, 15765.
- [111] L. J. Chen, Y. N. Li, J. Fan, H. K. Bisoyi, D. A. Weitz, Q. Li, *Adv. Opt. Mater.* **2014**, *2*, 845.
- [112] Z. G. Zheng, B. W. Liu, L. Zhou, W. Wang, W. Hu, D. Shen, *J. Mater. Chem. C* **2015**, *3*, 2462.